Self-renewing tissue-resident endothelial-macrophage progenitor cells originate from yolk sac and are a local source of inflammation and neovascularization in postnatal aorta

Running title: Yolk sac origins of postnatal tissue progenitor cells

Anna Williamson[1,2], Deborah Toledo-Flores[1,2], Sanuri Liyanage[1,2], Mohammadhossein Hassanshahi[1,2], Catherine Dimasi[1], Nisha Schwarz[1], Sanuja Fernando[1,2], Thalia Salagaras[1], Aaron Long[1,3], Belinda A. Di Bartolo[4], Jan Kazenwadel[5], Natasha L. Harvey[5], Grant R. Drummond[6], Antony Vinh[6], Vashe Chandrakanthan[7], Ashish Misra[8], Joanne T.M. Tan[1,2], Claudine S. Bonder[5], Stephen J. Nicholls[9], Christina A. Bursill[1,2], Peter J. Psaltis[1,2, 3 *]

[1] Vascular Research Centre, Heart and Vascular Program, Lifelong Health Theme, South Australian Health and Medical Research Institute, Adelaide, South Australia, 5000 Australia

[2] Adelaide Medical School, University of Adelaide, Adelaide, South Australia, 5000, Australia

[3] Department of Cardiology, Royal Adelaide Hospital, Central Adelaide Local Health Network, Adelaide, South Australia, 5000, Australia

[4] The Kolling Institute, The University of Sydney, St Leonards, New South Wales, 2064, Australia

[5] Centre for Cancer Biology, University of South Australia and SA Pathology, Adelaide, South Australia, 5000, Australia

[6] Department of Physiology, Anatomy and Microbiology and Centre for Cardiovascular Biology and Disease Research, School of Life Sciences, La Trobe University, Bundoora, Victoria, 3086, Australia.

[7] School of Medical Sciences, University of New South Wales, Sydney, New South Wales, 2052, Australia

[8] Heart Research Institute, Newtown, New South Wales, 2042, Australia

[9] Monash Cardiovascular Research Centre, Monash University, Clayton, Melbourne, Victoria, 3800, Australia

Address for Correspondence

Peter J. Psaltis, MBBS PhD

Vascular Research Centre, Lifelong Health Theme, Level 6

South Australian Health and Medical Research Institute

PO Box 11060, Adelaide, SA, 5001, Australia.

Tel: +61 8 8128 4534

Fax: +61 8 8362 2724

peter.psaltis@sahmri.com

SUMMARY

Converging evidence indicates that extra-embryonic yolk sac is the source of both macrophages and endothelial cells in adult mouse tissues. Prevailing views are that these yolk sac-derived cells are maintained after birth by proliferative self-renewal in their differentiated states. Here we identify clonogenic, self-renewing endothelial-macrophage (EndoMac) progenitor cells in postnatal mouse aorta, heart and lung, that are independent of definitive hematopoiesis and derive from a CX_3CR1^+ and $CSF1R^+$ yolk sac source. These bipotent progenitors are highly proliferative and vasculogenic, contributing to adventitial neovascularization in the aortic wall and forming perfused blood vessels after adoptive transfer into ischemic tissue. We establish a regulatory role for angiotensin II, which enhances their clonogenic, self-renewal and differentiation properties. Our findings demonstrate that tissue-resident EndoMac progenitors participate in local inflammatory and vasculogenic responses by contributing to the renewal and expansion of yolk sac-derived macrophages and endothelial cells postnatally.

KEYWORDS

Angiotensin II, CSF1R, CX_3CR1, Endothelial cell, Hemangioblast, Lineage mapping, Macrophage, Progenitor cell, Vasculogenesis, Yolk sac.

INTRODUCTION

Among diverse roles, macrophages are integral to development of blood and lymphatic vessels during normal organogenesis and responses to tissue injury, ischemia and other diseases (Cahill et al., 2021; Fantin et al., 2010; Gurevich et al., 2018; Qian and Pollard, 2010). They proliferate and assemble around neovessels, producing angiogenic factors and supporting endothelial anastomoses and vascular remodeling (Fantin et al., 2010). In return, endothelial cells help regulate the self-renewal of hematopoietic stem cells (HSCs) and their differentiation into macrophages (He et al., 2012). Understanding how macrophage-endothelial interactions arise is important to more effectively target inflammation and neovascularization in different pathophysiological conditions.

Historically, circulating monocytes were thought to be the source of tissue macrophages (van Furth and Cohn, 1968). Monocytes derive from definitive hematopoiesis, which originates embryonically with emergence of HSC clusters from the endothelium of the aorta-gonad-mesonephros (AGM) at around embryonic day (E) 10.5 in mice (Boisset et al., 2010; Medvinsky et al., 2011; Taoudi et al., 2008). These HSCs seed fetal liver before colonizing bone marrow (BM) perinatally, the main hematopoietic organ after birth (Medvinsky et al., 2011). Numerous studies have now established that HSC-monocyte ancestry does not account for all tissue macrophages (Ensan et al., 2016; Epelman et al., 2014; Ginhoux et al., 2010; Gomez Perdiguero et al., 2015; Hashimoto et al., 2013; Schulz et al., 2012; Yona et al., 2013). During embryogenesis, extra-embryonic yolk sac (YS) is the first site to produce macrophages via distinct developmental programs. This begins with primitive macrophage precursors in YS blood islands between E7.0 and E8.25 (Bertrand et al., 2005; Hoeffel and Ginhoux, 2018), followed by erythromyeloid progenitors (EMPs) which bud from specialized YS hemogenic endothelium (Kasaai et al., 2017) and comprise two waves (Hoeffel and

Ginhoux, 2018). From E7.5, early c-Kit^{+}CSF1R^{+} EMPs produce erythrocytes, megakaryocytes and YS macrophages in a process that is independent of the transcription factor, Myb (Gomez Perdiguero et al., 2015; Iturri et al., 2021; Schulz et al., 2012). This does not involve monocyte intermediates but rather sequential differentiation into CX_3CR1^{+} pre-macrophages and mature F4/80^{Hi} macrophages (Bertrand et al., 2005; Mass et al., 2016; McGrath et al., 2015; Palis et al., 1999). Macrophage progenitors, in both multipotent EMP and pre-macrophage stages, expand in YS and circulate to embryonic tissues to complete their maturation (Stremmel et al., 2018). This migration peaks around E10.5 and is mostly complete by E12.5. From E8.5, late Myb^{+}c-Kit^{+}CSF1R^{Lo} EMPs also differentiate into YS macrophages and traffic to liver, where they expand and generate lineage-specific hematopoietic progenitors and fetal blood cells, including monocytes (Hoeffel et al., 2015; McGrath et al., 2015).

Long-lived populations of YS-derived macrophages persist in adult tissues, including brain, skin, liver, heart, lung and aortic adventitia (Ensan et al., 2016; Epelman et al., 2014; Ginhoux et al., 2010; Gomez Perdiguero et al., 2015; Guilliams et al., 2013; Hashimoto et al., 2013; Schulz et al., 2012; Yona et al., 2013). These are maintained independently of BM hematopoiesis through local proliferation and seemingly, by self-renewal (Sieweke and Allen, 2013). With the exception of brain microglia that originate from the initial pool of YS-derived macrophages (Ginhoux et al., 2010), controversy remains as to whether other tissue macrophages are seeded from early EMPs (without monocyte intermediates) (Gomez Perdiguero et al., 2015) or late EMPs (via fetal liver monocytes) (Hoeffel et al., 2015).

Recent studies indicate that YS EMPs also contribute endothelial cells to the blood and lymphatic vessels of some organs (Cahill et al., 2021; Plein et al., 2018). Although disputed

(Feng et al., 2020), the possibility that EMPs produce both hematopoietic and endothelial cells is intriguing, especially given long-standing speculation around the embryonic existence of mesoderm-derived, bipotent hemangioblasts (Murray, 1932). While hemangioblasts have been shown to emerge during hemato-endothelial differentiation of pluripotent stem cells *in vitro* (Takata et al., 2017; Zambidis et al., 2008), their presence in postnatal tissues remains unproven (Psaltis and Simari, 2015). We previously identified that the adventitia of adult mouse arteries contains Sca-1$^+$CD45$^+$ progenitors, which selectively generate macrophage colony-forming units (CFU-M) in methylcellulose and produce macrophages and endothelial-lined neovessels after *in vivo* transfer (Psaltis et al., 2012; Psaltis et al., 2014; Toledo-Flores et al., 2019). As the adventitial Sca-1$^+$CD45$^+$ population is heterogeneous, our studies stopped short of claiming the bipotency of these progenitors at a clonal level. Here, we establish the identity of postnatal tissue-resident CFU-M progenitors as self-renewing, bipotent endothelial-macrophage (EndoMac) progenitor cells, that originate from an early YS source and are seeded in aorta, heart and lung during fetal development.

RESULTS

c-Kit, CX$_3$CR1 and CSF1R identify highly proliferative, self-renewing CFU-M progenitors in postnatal aorta

To establish the identity of CFU-M forming cells from mouse aorta, we cultured aortic digests from 12 week-old (w) C57BL/6J mice in methylcellulose (MethoCult GF M343, StemCell Technologies) for 14 days (d). This generated 17.0±12.0 CFU-M/10^5 cells (n=10), with colonies further classified based on size as ~72% small (~30-100 cells), ~27% medium (~100-1000) and <1% large (>1000) (**Figure 1A**). Re-culturing the content of primary (1°) cultures for another 14 d resulted in secondary (2°) CFU-M yield that was more than ~12-fold that of 1° cultures, indicating colony renewal and expansion (**Figure 1B**). To study this

further, we isolated individual 1° CFU-M and disaggregated each colony into single cell suspensions that were re-plated in separate wells. Importantly, this showed that CFU-M renewed from single cell origins, with 1 new colony produced per ~15 cells (**Figure 1C**).

Having established that CFU-M renew clonally, we used flow cytometry to identify their cellular composition. 1° CFU-M contained a homogeneous population that was negative for lineage (Lin) and monocyte/macrophage markers (CD11b, F4/80), but positive for CD45, Sca-1, c-Kit, CX_3CR1 and CSF1R (**Figure 1D**). This immunophenotype was similarly enriched in 2° CFU-M, confirming self-renewal (**Figure 1E**). CFU-M also expressed the hematopoietic progenitor and EMP markers, CD34, CD16/32, CD93 (AA4.1) and CD43 (Perdiguero et al., 2015), but not CD41 (very early-stage hematopoiesis), Flt3 (CD135) (definitive hematopoiesis) or Brachyury (hemangioblasts) (**Figure S1**). The stem cell marker, c-Myc, which regulates self-renewal was expressed on 25.0±5.4% cells, while Sox2, Nanog and Oct4 which are also associated with pluripotency, were negative. Apart from CX_3CR1 and CSF1R, other mature myeloid markers were negative (CCR2, CD206, CD86, MerTK, MHCII, Ly6C, Gr1) or lowly expressed (CD64, CD24). CFU-M were also negative for the lymphatic and macrophage marker, LYVE-1, the erythroid marker, Ter119, and the endothelial markers, CDH5 (CD144), VEGFR2 and TIE2, although they did express CD31, which is also found on myeloid progenitors (Bertrand et al., 2005). Importantly, we identified $Lin^-CD45^{+/Lo}CD11b^-F4/80^-c\text{-}Kit^+Sca\text{-}1^+CX_3CR1^+CSF1R^+$ progenitors in digests of C57BL/6 aorta (0.3±0.3% or 3270±2937 cells per aorta, n=20), mirroring the cell surface phenotype of cultured CFU-M (**Figure 1F**). Bromodeoxyuridine (BrdU) uptake revealed that these are actively proliferating, with three-fold more of these progenitors in S-phase of cycle than $CD11b^+F4/80^+$ macrophages (**Figure 1G**),

Fractalkine receptor, CX_3CR1, has been used to characterize tissue-resident macrophages, including those in adventitia, and to trace their embryonic origins (Ensan et al., 2016; Epelman et al., 2014; Yona et al., 2013). As CFU-M progenitors expressed CX_3CR1, we studied *Cx3cr1*$^{GFP/+}$ mice, which express green fluorescent protein (GFP) under control of the *Cx3cr1* locus (Jung et al., 2000). CFU-M from *Cx3cr1*$^{GFP/+}$ aortas were GFP$^+$ under fluorescence microscopy and flow cytometry (**Figure S2A**). Whereas other studies have focused on CX_3CR1 expression by aortic macrophages (Ensan et al., 2016), we also identified CX_3CR1^+c-Kit$^+$ progenitors in aortic adventitia (**Figure 1H**) and determined by flow cytometry that they account for 18.9±4.7% of CX_3CR1^+ cells in the aortic wall (n=6) (**Figure S2B**). Fluorescence activated cell sorting (FACS) of *Cx3cr1*$^{GFP/+}$ aortic cells showed that CFU-M forming capacity was restricted to GFP$^+$ (especially GFP^{Hi}) cells (**Figure S2C**), and specifically GFP$^+$CD11b$^-$F4/80$^-$ progenitors, not GFP$^+$CD11b$^+$F4/80$^+$ macrophages (**Figure 1I** and see **Figure S2D**).

As evidence of the functional importance of CX_3CR1, addition of its ligand, CX_3CL1, resulted in 1.6-fold higher CFU-M yield from aortic cells (**Figure 1J**), similar to the effect of macrophage colony-stimulating factor (M-CSF), the ligand for CSF1R (**Figure 1K**). We also compared *Cx3cr1*$^{GFP/+}$ mice to *Cx3cr1*$^{GFP/GFP}$ littermates, that lack both functional *Cx3cr1* alleles. *Cx3cr1*$^{GFP/GFP}$ aortas had almost four-fold lower CFU-M yield (**Figure 1L**) and contained ~60% fewer progenitors by flow cytometry (**Figure 1M**). Therefore CX_3CR1 is both a marker of self-renewing CFU-M progenitors and promotes their clonogenicity and prevalence in aorta.

Tissue CFU-M progenitors are independent of definitive hematopoiesis

C-C chemokine receptor 2 (CCR2), the cognate receptor for C-C chemokine ligand 2 (CCL2), has been used to differentiate between monocyte-derived ($CCR2^+$) and locally maintained, embryonically derived ($CCR2^-$) macrophages in some tissues (Dick et al., 2019). Unlike CX_3CR1, CCR2 was not expressed on aortic CFU-M progenitors (**Figure S2E**). Aortic cells from *Ccr2*$^{-/-}$ mice formed more CFU-M than wildtype littermates, with a trend toward higher progenitor counts, despite fewer circulating monocytes (**Figures S2F-S2H**). Similarly, a disconnect between blood monocyte and aortic progenitor numbers was also seen when clodronate liposomes were used to deplete monocytes, suggesting independence between the two (**Figures S2I-S2K**).

These results led us to examine the relationship between CFU-M progenitors and definitive BM hematopoiesis by using *Flt3*^{Cre} x *Rosa*$^{mT/mG}$ mice. BM HSCs transiently upregulate the receptor tyrosine kinase Flt3 during hematopoietic differentiation (Karsunky et al., 2003). In *Flt3*^{Cre} x *Rosa*$^{mT/mG}$ mice, cells that originate from definitive hematopoiesis express GFP (Flt3-Cre$^+$), while those that do not are GFP$^-$ and express tdTomato (tdTom) (Flt3-Cre$^-$). Using these and C57BL/6 mice, we identified that digests of heart and lung also produce CFU-M that contain progenitors with the same immunophenotype as aorta (**Figures S3A-S3C**). CFU-M from all three tissues from *Flt3*^{Cre} x *Rosa*$^{mT/mG}$ mice were >95% Flt3-Cre$^-$, while BM produced a mixture of CFU-M and non-macrophage colonies that were >90% Flt3-Cre$^+$ (**Figures 2A-2B**). Similarly, although blood monocytes and Lin$^-$c-Kit$^+$Sca-1$^+$ BM HSCs were Flt3-Cre$^+$ (**Figures S3D-S3E**), aorta, heart and lung contained Lin$^-$CD45$^{+/Lo}$CD11b$^-$ F4/80$^-$Sca-1$^+$c-Kit$^+$ progenitors that were predominantly Flt3-Cre$^-$ (**Figure 2C**). In keeping with other studies (Ensan et al., 2016; Epelman et al., 2014), these tissues also contained both Flt3-Cre$^+$ and Flt3-Cre$^-$ macrophages, whereas BM macrophages were predominantly Flt3-

Cre^{+} and brain microglia Flt3-Cre^{-} (**Figure S3F**). Together, these results show that postnatal tissue CFU-M progenitors are not derived from definitive hematopoiesis.

Tissue CFU-M progenitors are seeded embryonically

To elucidate the origins of tissue CFU-M progenitors, we next performed age profiling after birth. Aortic CFU-M yield was ~10-fold higher from P1 (postnatal day 1) than 3 w and 12 w mice, and lowest from 52 w mice (**Figure 2D**). P1 CFU-M formed more quickly, comprised more medium and large colonies and had greater capacity for self-renewal (**Figures S4A-S4B**). Flow cytometry supported the higher abundance of progenitors in P1 aorta and their declining prevalence as mice age (**Figure 2E**). Similar results were obtained for heart and lung (**Figures S4C-S4G**).

As tissue CFU-M progenitors are present at birth, we examined their emergence during embryonic development. CFU-M grew from digests of YS, beginning around E7.5 and with higher yield from E8.5 onwards (**Figure 2F**). They made up 99% of all colonies grown from YS at E7.5, 90% at E8.5 and 85% at E9.5 (**Figure S4H**). YS CFU-M from *Cx3cr1*$^{GFP/+}$ embryos expressed the same surface marker phenotype as CFU-M from postnatal tissues (**Figure 2G**) and were negative for Flt3 (**Figure S4I**). Compared to adult aortic CFU-M, YS CFU-M were larger in size (**Figure S4G**), with higher self-renewal capacity (**Figure S4B**) and higher expression of Sox2 and c-Myc, suggesting a more primitive state (**Figure S4I**). Although CFU-M did not grow from digests of whole embryo at E8.5 or E9.5, they formed from AGM, heart and brain from E10.5 onwards (**Figure 2F**). Coinciding with the emergence of definitive HSCs from dorsal aorta at ~E10.5-11.5 (Medvinsky et al., 2011), we also observed non-macrophage colonies (G, granulocyte; GM, granulocyte-macrophage; GEMM, granulocyte-erythrocyte-monocyte-megakaryocyte; BFU-E, burst-forming units-

erythroid) from AGM during this gestational window (**Figure S4J**). However, unlike CFU-M these disappeared by E12.5. Colony growth from liver increased between E10.5 and E11.5 and consisted mostly of non-macrophage colonies through to E15.5, consistent with seeding of HSCs and multipotent progenitors from AGM and YS (Hoeffel et al., 2015; McGrath et al., 2015) (**Figure S4K**).

Flow cytometry showed a similar time-course for the appearance of $CD45^{+/Lo}$c-$Kit^{+}CX_3CR1^{+}$ cells in YS from E8.5 and AGM from E10.5 (**Figures 2H-2I**), while confocal microscopy identified c-$Kit^{+}CX_3CR1^{+}$ progenitors in aortic adventitia at E12.5 and E15.5 (i.e. after disappearance of definitive HSCs from AGM) (**Figure 2J**), as well as in heart and lung (**Figure S4L**).

Tissue CFU-M progenitors originate from CX_3CR1^{+} and $CSF1R^{+}$ YS progenitors

Murine aortic adventitia has been shown to contain locally maintained macrophages derived from CX_3CR1^{+} and $CSF1R^{+}$ YS progenitors (Ensan et al., 2016; Weinberger et al., 2020). As CFU-M progenitors appear in YS before AGM, we used timed fate-mapping approaches to confirm their YS origins. Female *Cx3cr1*$^{\text{CreER-YFP}}$ mice, which express Cre recombinase under control of the *Cx3cr1* promoter upon exposure to 4-hydroxytamoxifen (TAM), were crossed to male *Rosa*^{tdTom} mice (Ensan et al., 2016). Pregnant dams were administered TAM at E8.5 or E9.5 to induce irreversible expression of the tdTom reporter in YS CX_3CR1^{+} cells and their progeny. Tissues from offspring were examined at E15.5, P1 and 12 w for $tdTom^{+}$ labeling, which was normalized to brain microglia that are YS-derived (Schulz et al., 2012) (**Figure 3A**). Although TAM induction at E8.5 resulted in minimal $tdTom^{+}$ expression (not shown), induction at E9.5 led to robust $tdTom^{+}$ labeling of microglia (**Figure S5A**). Unlike colonies from E15.5 liver and adult BM that were $tdTom^{-}$, CFU-M from aorta, heart and lung

were tdTom$^+$ and exclusively derived from an E9.5 CX$_3$CR1$^+$ source (**Figures 3B** and **S5B**). Whereas previous studies have focused on the macrophage (Ensan et al., 2016; Epelman et al., 2014; Schulz et al., 2012) or endothelial fate (Feng et al., 2020; Plein et al., 2018) of YS progenitors, we tracked both lineages together with CFU-M progenitors. E9.5 CX$_3$CR1$^+$ cells gave rise to all three cell types in aorta, heart and lung (**Figures 3C-3D** and **S5B-S5F**). Progenitors made up the highest number of tdTom$^+$ cells in E15.5 AGM, followed by endothelial cells and lastly macrophages. After birth, the proportions of YS-derived endothelium and macrophages in aorta both increased, with reduction in progenitors (**Figures 3C-3D**). By comparison, endothelial cells were the predominant tdTom$^+$ population at each age studied in heart and in 12 w lung (**Figures S5D-S5F**).

Complementary fate-mapping was performed by giving TAM to *Csf1r*^{MerCreMer} x *Rosa*$^{mT/mG}$ mice at E8.5 to induce GFP expression in YS CSF1R$^+$ cells, including EMPs and their progeny (Epelman et al., 2014) (**Figure 3E**). CFU-M from 12 w aorta, heart and lung showed 100% GFP labeling normalized to microglia, as distinct from BM colonies that were GFP$^-$ (**Figures 3F** and **S5G-S5H**). Flow cytometry identified GFP$^+$ progenitors, macrophages and endothelial cells in adult aorta, heart and lung, with endothelial cells again being most prevalent in each tissue (**Figures 3G-3H** and **S5J-S5K**). Confocal microscopy also demonstrated GFP$^+$ YS-derived cells in adult aorta (**Figure 3I**), comprising each of these three cell types (**Figure 3J**). We then used FACS to isolate GFP$^+$ progenitors, macrophages and endothelial cells to high purity from the aortas of these 12 w mice (**Figure 3K**). Wright-Giemsa staining showed that progenitors had rounded morphology with smooth surface membrane and lacked the protrusions and intracellular vacuolations of macrophages (**Figure 3L**), thus resembling the morphology reported for c-Kit$^+$AA4.1$^+$CD45^{Lo} EMPs and CX$_3$CR1$^+$ pre-macrophages in YS (Mass et al., 2016). Although they had similarly sized nuclei as

macrophages, progenitors had less cytoplasm and a higher nuclear:cell area ratio (**Figure 3L**). Critically, CFU-M were only produced by progenitors and not YS-derived macrophages or endothelial cells after culture in methylcellulose (**Figure 3M**). These data establish that tissue-resident CFU-M progenitors originate from YS EMPs and are seeded embryonically.

CFU-M progenitors have bipotent endothelial-macrophage plasticity

The diminution in YS-derived progenitors in aorta after birth countered by increases in YS-derived macrophages and endothelial cells (**Figure 3C**), led us to examine whether progenitors differentiate into these lineages to contribute to their postnatal expansion and maintenance. FACS-isolated progenitors, macrophages and endothelial cells from aorta were cultured in Matrigel^{TM} to compare their angiogenic capacity *in vitro*. While macrophages produced no vascular-like cords, progenitor and endothelial cells formed cord networks of different morphologies, but similar length cords (**Figure 4A**). Progenitors assembled in clusters by day 3 (data not shown) before producing complex interconnected cords by day 7. Whereas flow cytometry showed that cord networks from endothelial cultures only contained endothelial cells (**Figure 4B**), networks produced by progenitors consisted of macrophages and endothelial cells, with some residual progenitor cells (**Figure 4C**).

The Matrigel^{TM} assay was repeated using progenitors from culture-derived aortic CFU-M. Progenitors from individual colonies again formed similar networks comprising both endothelial cells and macrophages, confirming that they are bipotent at a clonal level (**Figures 4D-4E**). Newly produced macrophages were mostly LYVE-1^{+}, MHCII^{-}, CX$_3$CR1^{+} and CCR2^{-} (**Figure 4E** and **Table S1**), consistent with the surface marker profile of YS-derived tissue macrophages (Ensan et al., 2016; Epelman et al., 2014). Macrophage and endothelial transformation of progenitors was also confirmed by showing new capacity to

take up oxidized and acetylated LDL, respectively (**Figures 4F-4G**). Angiogenic capacity was highest for CFU-M progenitors from E9.5 YS and P1 aorta and lower from 12 w and 52 w aorta (**Figure 4H**).

We next examined whether aortic CFU-M progenitors mediate adventitial neovascularization, as occurs during *vasa vasorum* expansion. Aortic ring assays were performed from E9.5 TAM-induced 12 w *Cx3cr1*$^{CreER\text{-}YFP}$ x *Rosa*^{tdTom} mice and produced YS-derived tdTom^{+} sprouts (**Figures S6A-S6B**), with seven-fold higher content of tdTom^{+} cells compared to whole aorta, as measured by flow cytometry (**Figure S6C**). tdTom^{+} sprouts contained endothelial cells, progenitors and macrophages (mostly CX$_3$CR1^{+}LYVE-1^{+}MHCII^{-}) in decreasing order of abundance (**Figures S6D**). Similar results were obtained from E8.5 TAM-induced 12 w *Csf1r*^{MerCreMer} x *Rosa*$^{mT/mG}$ mice (**Table S2**). Finally, we used aortic rings from C57BL/6 mice, in which adventitia had been removed to eliminate sprouting (**Figure 4I**). Seeding aortic CFU-M progenitors from ubiquitous GFP mice rescued adventitial angiogenesis with formation of GFP^{+} sprouts, that contained endothelial cells and predominantly LYVE-1^{+}MHCII^{-} macrophages (**Figures 4J-4K** and **Table S1**). Therefore YS-derived progenitors participate in adventitial neovascularization, by producing both endothelial cells and macrophages.

To study the fate and vasculogenic capacity of CFU-M progenitors *in vivo*, we performed adoptive cell transfer experiments. Surgery was performed on 12 w C57BL/6 mice to induce hindlimb ischemia (Toledo-Flores et al., 2019), before injecting the quadriceps and gastrocnemius with CFU-M-derived progenitors from 12 w aorta or E9.5 YS from GFP mice (~1.5x10^{4} cells) or cell-free Matrigel^{TM} (**Figures 5A** and **S6E**). Laser Doppler imaging showed that aortic progenitors improved perfusion recovery over 14 d compared to control

(**Figure 5B**), accompanied by increased capillary and arteriolar density in injected muscle (**Figure S6E**). At day 14, GFP^+ cells were detected in recipient muscle but not peripheral blood, with flow cytometry revealing that donor progenitors had produced new endothelial cells and macrophages (**Figure 5C** and **Table S1**). Confocal microscopy identified host-perfused, GFP^+ endothelial-lined neovessels, with adjacent clusters of GFP^+ $CD68^+$ macrophages (**Figure 5D**). Similar results for perfusion recovery and endothelial and macrophage fate were obtained after injection of YS progenitors (**Figures S6F-H**).

Collectively, the above results identify CFU-M progenitors as vasculogenic bipotent EndoMac progenitors. We next examined their self-renewal capacity and the durability of their progeny *in vivo*. Digests of quadriceps and gastrocnemius were prepared from C57BL/6 mice 14 d after injection of GFP^+ aortic progenitors. They generated GFP^+ CFU-M in methylcellulose-based culture from which GFP^+ progenitors were isolated and used in 2° hindlimb transfer studies (**Figure 5E**). After another 14 d, engrafted GFP^+ cells had mostly transformed into endothelial cells or macrophages, with few remaining progenitors (**Figure 5F**). Similar results were obtained in 1° transfer studies that were followed for eight weeks instead of two (**Figures 5G** and **5H**). These results show that while aortic progenitors produce durable endothelial and macrophage progeny, their own numbers diminish over time indicating that their capacity for self-renewal is finite.

Regulatory effects of Angiotensin II on aortic EndoMac progenitors

The renin-angiotensin system, and specifically angiotensin II (AngII), play key regulatory roles in myelopoiesis (Lin et al., 2011; Shen and Bernstein, 2011) and vascular inflammation (Moore et al., 2015; Weinberger et al., 2020). When pluripotent stem cells undergo hemato-endothelial differentiation *in vitro*, they transition through bipotent hemangioblasts that form

colonies and express ACE (CD143) and the receptors for AngII, ATR1 and ATR2 (Zambidis et al., 2008). We found that ACE was expressed on EndoMac progenitors from aortic CFU-M in culture (86.9±6.7%, n=5), fresh aortic digests (85.9±11.0%, n=5) and CFU-M from YS (99.8±0.05%, n=3) (**Figures 6A-6C**). Aortic progenitors also expressed ATR1 (87.4±1.2%, n=3) and ATR2 (84.9±13.5%, n=3) at surface protein (**Figure 6A**) and mRNA level (**Figure 6D**). AngII induced concentration-dependent increases in 1° CFU-M yield from aortic cells (**Figure 6E**) and at 100 nM stimulated CFU-M to self-renew for four passages (**Figure 6F**). Treatment with inhibitors of ACE (enalapril), ATR1 (losartan) and ATR2 (PD123,319) showed that inhibition of ATR1 and ATR2 reduced aortic CFU-M yield (**Figure 6G**). To study the effect of AngII on differentiation, we injected 10^4 GFP^+ aortic progenitors into the peritoneum of C57BL/6 mice and assessed their fate by flow cytometry 72 h later (**Figures 6H-6J**). Daily *i.p.* injections of AngII promoted expansion of progenitor-derived macrophages by 14.5-fold and 3.4-fold compared to PBS and M-CSF, respectively (**Figures 6J-6K**). In keeping with these different effects on EndoMac progenitors, qPCR showed that AngII upregulated mRNA levels of genes involved in cell division (*Ccna1*, *Ccnb1*, *Ccnd2*), self-renewal (*Myc*, *Nanog*, *Klf4*) (Satoh et al., 2004; Soucie et al., 2016), myelopoiesis (*Klf4*, *Irf8*) (Li et al., 2011), M2-like macrophage polarization (*Arg1*) and endothelial specification and angiogenesis (*Cdh5*, *Cd248*) (**Figures 6L-6P**).

YS-derived EndoMac progenitors expand early and contribute to AngII-induced vascular inflammation

AngII-induced vascular inflammation is characterized by expansion of adventitial macrophages (Rateri et al., 2011), adventitial fibrosis (Wu et al., 2016) and in some mouse strains, development of aortic aneurysms (Daugherty et al., 2000). A recent study reported that after 10 d of exposure to AngII, adventitial macrophages expanded due to both

recruitment of BM-derived cells and local proliferation of embryonic-derived macrophages (Weinberger et al., 2020). As AngII induced progenitor expansion and differentiation to macrophages within 72 h in our peritoneal transfer assay, we focused on its early effects on aortic progenitors and macrophages after systemic infusion by osmotic pump. In *Flt3*^{Cre} x *Rosa*$^{mT/mG}$ mice, 48 h of AngII caused increases in both Flt3-Cre^{+} and Flt3-Cre^{-} macrophages compared to PBS control (2.9 and 5.8-fold, respectively) (**Figures 7A**, **7B**), with more Flt3-Cre^{+} and Flt3-Cre^{-} macrophages in S-phase of cycle (both 2.9-fold vs PBS) (**Figure 7C**). As a potential contributor to the expansion of non-BM derived macrophages, AngII also induced expansion and proliferation of Flt3-Cre^{-} progenitors, with fold comparisons compared to PBS: 3.0x for aortic CFU-M yield (**Figure 7D**); 8.5x for progenitor number assessed by flow cytometry (**Figure 7E**); and 10.5x for progenitors in S-phase (**Figure 7F**).

We next used adult *Cx3cr1*$^{CreER-YFP}$ x *Rosa*^{tdTom} mice that had been administered TAM at E9.5. AngII or PBS were infused by osmotic pump for 12 h, 48 h or 168 h (7 d) (**Figure 7G**). AngII increased the numbers of tdTom^{+} cells in aorta at all three time-points compared to PBS (fold comparisons by flow cytometry: 1.7x at 12 h, 1.8x at 48 h, 2.9x at 168 h) (**Figure 7H**). This was supported by confocal microscopy analysis of sections of descending aorta at 48 h (**Figures 7I** and **S7A**). As measured by CFU-M yield, the AngII-induced expansion of EndoMac progenitors was highest at 12 h (6.1-fold vs PBS), still evident at 48 h (3.3-fold) but no longer at 168 h (1.3-fold) (**Figure 7J**). We also used a strategy of BrdU pulse-chase in these mice to test for an ancestral relationship between YS-derived progenitors, macrophages and endothelium in aorta under AngII-induced inflammation. BrdU was injected 11 h after the start of AngII or PBS, with aortas studied at the same three time-points of infusion as above (**Figure 7G**). Progenitors were by far the most proliferative YS-derived population in both PBS and AngII groups after 12 h of treatment (**Figure 7K**). As the number of

BrdU$^+$ tdTom$^+$ cells remained relatively constant over the study duration (**Figures 7L-7M**), we analyzed how BrdU labeling was distributed across different YS-derived populations over time. Whereas it was highest in progenitors at 12 h and diminished thereafter (**Figure 7N**), it progressively increased in tdTom$^+$ macrophages and endothelial cells in AngII aortas, peaking in both at 168 h (**Figures 7O-7P**). A similar pattern of redistribution of BrdU labeling was seen among GFP$^+$ YS-derived cells over 14 d of pulse-chase in steady state aortas from E8.5 TAM-induced 12 w *Csf1r*^{MerCreMer} x *Rosa*$^{mT/mG}$ mice (**Figures S7B-I**). Together with our earlier results, these findings support a model whereby YS-derived progenitors undergo very early proliferative expansion in response to AngII, followed by differentiation into macrophages and endothelium.

DISCUSSION

The intimate association between the hematopoietic and endothelial lineages begins early in development. Converging evidence indicates that YS EMPs give rise to both macrophages and endothelial cells in adult mouse tissues (Gomez Perdiguero et al., 2015; Plein et al., 2018). In this study we identify and characterize undifferentiated EndoMac progenitors in murine aorta, heart and lung that also originate from a YS source. These progenitors are more abundant at birth, at which time they have enhanced clonal and self-renewal capacity and are maintained independently of definitive hematopoiesis. As shown by differentiation, adoptive transfer and BrdU pulse-chase studies, they are bipotent for macrophage and endothelial lineages and possess vasculogenic capacity. In association with expression of the hemangioblastic markers, ACE, AT1R and AT2R, we demonstrate a pathophysiologically relevant regulatory role for AngII, which rapidly stimulates their clonogenic, self-renewal and differentiation properties.

Most mature cell types rely on the self-renewal of stem cells and proliferation and differentiation of transient amplifying progenitors for their homeostatic turnover and recovery after tissue insult. Although there has been conjecture about how embryonically derived macrophages are maintained after birth, prevailing opinion favors their ability to self-renew without losing functional or differentiated status (Sieweke and Allen, 2013). This was initially based on experiments showing self-renewal of macrophages in which MafB and c-Maf were genetically knocked out (Aziz et al., 2009). Subsequent studies have provided contrasting data either supporting the long-lived nature of tissue-resident macrophages, especially microglia (Reu et al., 2017), their stochastic turnover (Hashimoto et al., 2013; Huang et al., 2018), repopulation by clonal expansion (Ghigo et al., 2013; Tay et al., 2017) or differentiation from local progenitors (Elmore et al., 2014). The mechanistic basis for macrophage self-renewal has been linked to downregulation of MafB/cMaf, which occurs constitutively in some macrophage populations (e.g. alveolar macrophages) or can be induced (e.g. by M-CSF). This in turn activates a self-renewal gene network, centered around *Myc*, *Klf2* and *Klf4* (Soucie et al., 2016). Evidence that embryonically derived macrophages undergo *bona fide* self-renewal in aorta and heart is somewhat circumstantial and includes the persistent labeling of some macrophage subtypes after postnatal induction of fate-mapping in *Cx3cr1*^{CreER} and *Csf1r*^{MerCreMer} reporter mice (Dick et al., 2019; Ensan et al., 2016). However**,** these results are also compatible with the turnover and differentiation of previously unrecognized EndoMac progenitors, which express CX_3CR1 and CSF1R.

As shown here, growth of CFU-M from adult tissues is not due to clonal proliferation of monocytes or macrophages, but rather YS-derived progenitors. The finding that CFU-M undergo self-renewal from single cell origins paved the way for us to study their composition and uncover a unique $Lin^{-}CD45^{+/Lo}CD11b^{-}F4/80^{-}Sca\text{-}1^{+}c\text{-}Kit^{+}CX_3CR1^{+}CSF1R^{+}$ fingerprint,

that identifies progenitors in both digested tissue and culture-derived CFU-M. This surface phenotype distinguishes EndoMac progenitors from BM HSCs and their lineage-committed progenitors, such as macrophage/dendritic cell progenitors and common monocyte progenitors, which lack Sca-1 but express Flt3/CD135 and Ly6C, respectively (Auffray et al., 2009; Hettinger et al., 2013). As a relatively high percentage of progenitors are actively dividing even in steady state, it is not surprising that their ability to self-renew is finite and diminishes with aging, along with their clonogenic and angiogenic capacity. Combined with a lack of circulatory renewal from BM HSCs, this helps explain why tissue progenitor numbers decrease postnatally at a faster rate than their less proliferative, durable endothelial and macrophage progeny. However, we also demonstrate that their proliferation and self-renewal can be amplified by stimulatory cues, such as elicited by AngII.

As in previous studies (Samokhvalov et al., 2007), we found negligible contribution from YS to the adult HSC pool. As revealed by embryonic profiling across different gestational ages and timed induction of fate-mapping, EndoMac progenitors emerge in YS around E7.5-E8.5 and expand there until E10.5, by which time they have migrated intra-embryonically to AGM, heart and other tissues. This aligns with prior findings for multipotent EMPs and CX_3CR1^+ pre-macrophages (Stremmel et al., 2018). Throughout our differentiation assays, EndoMac progenitors adopted the fast-track pathway of macrophage differentiation characteristic of early YS EMPs, producing macrophages without passing through a monocyte intermediate stage. This separates them from late EMPs that colonize fetal liver where they produce monocytes and other lineage-committed progenitors (Hoeffel et al., 2015). This was reflected here by mixed growth of different CFU types from E12.5-15.5 liver, as distinct from selective CFU-M growth from AGM and heart at the same ages. Whereas the multipotency of YS EMPs includes primitive erythroid cells, megakaryocytes,

mast cells and neutrophils (Gentek et al., 2018; Iturri et al., 2021; McGrath et al., 2015), we found no evidence that postnatal EndoMac progenitors produce these lineages (not shown). Their differentiation capacity for macrophages and endothelium is therefore positioned between that of EMPs (McGrath et al., 2015; Plein et al., 2018) and pre-macrophages in YS (Mass et al., 2016). Consistent with this, they have an intermediate surface marker phenotype that retains expression of the early EMP markers, c-Kit, CSF1R, AA4.1, CD16/32 and CD45 (Lo) but not CD41, while acquiring the pre-macrophage marker, CX_3CR1. By comparison, pre-macrophages are otherwise characterized as $CD45^+$c-Kit^-CD11b^{Lo} (Mass et al., 2016).

The classical origin of embryonic vascular endothelial cells is the differentiation of mesoderm-derived angioblasts around E7.0 YS in mice (Potente et al., 2011). Subsequently, endothelial cells undergo local proliferation during tissue angiogenesis, with evidence for clonal expansion in adult tissues, such as heart and muscle under ischemic insult (Manavski et al., 2018). Other identified sources of postnatal endothelial renewal include circulating endothelial progenitor cells (Asahara et al., 1999) and tissue-resident endovascular progenitors (Patel et al., 2017). Plein *et al*. recently reported that endothelial cells in YS and some embryonic and adult tissues also derive from YS EMPs (Plein et al., 2018), although this was not reproduced by another study that used alternative lineage mapping techniques (Feng et al., 2020). In tracking the fate of early YS CX_3CR1^+ and $CSF1R^+$ progenitors, we examined both their macrophage and endothelial progeny through the lens of EndoMac progenitors. While endothelial cells were the most abundant lineage labeled in heart at each of the three ages studied, E15.5 aorta contained a predominance of YS-derived progenitors, that were replaced after birth by increasing numbers of macrophages and endothelial cells. In addition to the self-renewal of YS-derived macrophages and endothelium, another feasible explanation for this finding is the postnatal transformation of progenitors into these two

distinct lineages. We consistently observed this to occur across different *in vitro*, *in vivo* and BrdU pulse-chase studies, which also highlighted the highly proliferative nature of the progenitor population. Although our results suggest a differentiation bias toward the endothelial lineage in the settings of post-ischemia repair and *in vitro* angiogenesis, these progenitors can also rapidly generate macrophages, as seen after peritoneal injection. Importantly, they appear predisposed to forming macrophages that are LYVE-1^{+}MHCII$^{-/Lo}$CCR2^{-}, consistent with the identity of YS-derived macrophages that reside in heart and adventitia (Dick et al., 2019; Ensan et al., 2016; Weinberger et al., 2020).

The century-old notion of the hemangioblast, a bipotent progenitor for endothelial and hematopoietic cells in development (Murray, 1932), has been supported by *in vitro* evidence of a common pathway of hemato-endothelial differentiation from pluripotent stem cells (Kennedy et al., 2007; Takata et al., 2017; Zambidis et al., 2008). Given their macrophage-restricted hematopoietic potential and lack of expression of the canonical hemangioblast marker, Brachyury, we do not propose that EndoMac progenitors are *bona fide* hemangioblasts. However, their expression of other hemangioblast markers, namely ACE and both AngII receptor subtypes (Zambidis et al., 2008), focused our attention on AngII as a regulator of their properties within adult vasculature. AngII stimulated the proliferative, clonogenic, self-renewal and macrophage-forming capacity of aortic EndoMac progenitors, and upregulated relevant genes, such as *Nanog*, *Myc*, *Irf8* and *Arg1*. Together with our results from short-term AngII infusion in *Flt3*^{Cre} and *Cx3cr1*^{CreER} mice, this indicates that these progenitors are primed to provide an immediate proliferative response to AngII, that helps to feed the expansion of YS-derived adventitial macrophages and endothelial cells. As shown here and in another recent study (Weinberger et al., 2020), this is complemented by

recruitment and proliferation of BM-derived macrophages, which also contribute to AngII-induced adventitial inflammation.

In conclusion, our discovery of EndoMac progenitors adds to the recognized fate of YS EMPs in embryonic and postnatal tissues. Our findings demonstrate that these YS-derived progenitors provide a local source of macrophage and endothelial renewal that can be rapidly switched on during the early phases of tissue inflammation and neovascularization postnatally.

ACKNOWLEDGEMENTS

The authors thank Adelaide Microscopy at the University of Adelaide and staff of the Bioresources Facility and Flow Cytometry Core Laboratory of the South Australian Health and Medical Research Institute.

This work was supported by the National Health and Medical Research Council of Australia [PG 1086796, IG 2001541, PRF 1111630 to S.J.N., CDF 1161506 to P.J.P.]; the National Heart Foundation of Australia [VG 102981, Lin Huddleston Fellowship to C.A.B., FLF 100412 and 102056 to P.J.P.]; and the Royal Australasian College of Physicians.

AUTHOR CONTRIBUTIONS

Conceptualization, A.W., D. T-F., and P.J.P.; Investigation, A.W., D. T-F., S.L., M.H., C.D., N. S., S.F., T.S., A.L., B.A.D.B., J.K., N.L.H., G.R.D., A.V., V.C., A.M., J.T.M.T. and P.J.P.; Writing – Original draft, A.W. and P.J.P.; Writing – Review & Editing, A.W., N.L.H., G.R.D., V.C., J.T.M.T., C.S.B., S.J.N, C.A.B. and P.J.P.; Supervision, C.S.B., C.A.B. and P.J.P.; Funding acquisition, P.J.P..

DECLARATION OF INTERESTS

S.J.N. has received research support from AstraZeneca, Amgen, Anthera, Eli Lilly, Esperion, Novartis, Cerenis, The Medicines Company, Resverlogix, InfraReDx, Roche, Sanofi-Regeneron and Liposcience and is a consultant for AstraZeneca, Akcea, Eli Lilly, Anthera, Kowa, Omthera, Merck, Takeda, Resverlogix, Sanofi-Regeneron, CSL Behring, Esperion and Boehringer Ingelheim. P.J.P. has received research support from Abbott Vascular, consulting fees from Amgen and Esperion and speaker honoraria from AstraZeneca, Bayer, Boehringer Ingelheim, Merck Schering-Plough, Pfizer, Novartis and Sanofi.

SUPPLEMENTAL MATERIAL

Supplemental Methods

Tables S1-S4

Figures S1-S7

FIGURE LEGENDS

Figure 1. c-Kit, CX_3CR1 and CSF1R identify self-renewing aortic CFU-M progenitors.

(A) Examples of small, medium and large CFU-M from 12 w C57BL/6 aortic cells. Pie chart shows breakdown of CFU-M by colony size (n=5).

(B) Donor-matched primary (1°) and secondary (2°) CFU-M yield from 12 w C57BL/6 aorta (n=10). Paired t-test.

(C) Self-renewal of 2° CFU-M from single cell obtained from 1° CFU-M.

(D, E) Flow cytometry of cells from (D) 1° (n=3) and (E) 2° aortic CFU-M (n=4). Blue histogram, sample. Dotted, FMO control.

(F) Flow cytometry of aortic digest shows progenitor population (n=4).

(G) Flow cytometry of bromodeoxyuridine (BrdU) versus 7-aminoactinomycin (7-AAD) gated from aortic progenitors. Dotted box, S-phase. Percentages of progenitors (Prog) and macrophages (M□) in S-phase from 12 w C57BL/6 aorta (n=5). Paired t-test.

(H) Confocal microscopy of descending aorta from 12 w *Cx3cr1*$^{GFP/+}$ mouse shows adventitial (Ad) CX_3CR1^+c-Kit$^+$ progenitors. L, lumen.

(I) CFU-M yield from FACS-sorted aortic populations from 12 w *Cx3cr1*$^{GFP/+}$ mice (two experiments, six aortas each). N/A, not applicable.

(J, K) CFU-M yield from 12 w C57BL/6 aortic cells in presence of (J) 100 nM CX_3CL1 or (K) 50 nM M-CSF (n=6). Paired t-tests.

(L, M) Frequency of (L) CFU-M and (M) progenitors from aortas of 12 w *Cx3cr1*$^{GFP/+}$ and *Cx3cr1*$^{GFP/GFP}$ mice (n=7-10). Unpaired t-tests.

Data summarized as mean±SD.

Scale bar, 100 μm in (A), (C) and (H).

Also see Figures S1 and S2.

Figure 2. Tissue CFU-M progenitors are seeded embryonically and are independent of Flt3^{+} hematopoiesis.

(A) Light and fluorescence microscopy of CFU-M from aorta, heart, lung and BM of adult *Flt3*^{Cre} x *Rosa*$^{mT/mG}$ mice. Graph of Flt3^{+} and Flt3^{-} CFU-M yield from different tissues (n=5). Spl, spleen. Paired t-tests for each tissue.

(B) GFP and tdTom expression of cells in CFU-M from *Flt3*^{Cre} x *Rosa*$^{mT/mG}$ BM and aorta.

(C) Flow cytometry plots show Flt3^{-} progenitors (maroon) in aorta, heart and lung of *Flt3*^{Cre} x *Rosa*$^{mT/mG}$ mice. Blue dots, macrophages. Percentages represent mean of n=4.

(D, E) Age comparisons of (D) CFU-M yield (Kruskal-Wallis) and (E) number of progenitors (one-way ANOVA) for C57BL/6 aortas (n=3-6). Multiple comparison tests: *$p<0.05$ for 3 w vs 52 w; †$p<0.01$ and #$p<0.0001$ for comparison to P1.

(F) CFU-M yield from different tissues of *Cx3cr1*$^{GFP/+}$ mice at different embryonic ages (n=3-9).

(G) Flow cytometry of cells from YS CFU-M (n= 3).

(H) Flow cytometry of digests of YS, whole embryo and AGM from *Cx3cr1*$^{GFP/+}$ mice at different embryonic ages show $CX_3CR1^{+}CD45^{+/Lo}$c-Kit^{+} progenitors (n=3-5).

(I) Number of progenitors in YS, whole embryo or AGM at different embryonic ages (n=3-5).

(J) Confocal microscopy of E12.5 and E15.5 AGM from *Cx3cr1*$^{GFP/+}$ mice shows adventitial CX_3CR1^{+}c-Kit^{+} progenitors (arrows). L, lumen.

Data summarized as mean or mean±SD.

Scale bar, 100 µm in (A), (G) and (K).

Also see Figure S3 and S4.

Figure 3. CX_3CR1^+ and $CSF1R^+$ YS cells give rise to progenitors, macrophages and endothelial cells in aorta.

(A) E9.5 4-hydroxytamoxifen (TAM)-induced labeling of *Cx3cr1*$^{CreER\text{-}YFP}$ x *Rosa*^{tdTom} mice, with analysis at E15.5, P1 or 12 w.

(B) $tdTom^+$ CFU-M from 12 w aorta. Graph shows $tdTom^+$ vs $tdTom^-$ status of CFU-M from different tissues and ages, with results normalized to brain microglia (n=4). Ao, aorta. F. Li, fetal liver.

(C) Numbers of $tdTom^+$ progenitors (prog), macrophages (M□) and endothelial cells (EC) in AGM/aorta at different ages (n=3 for E15.5 and 12 w and n=4 for P1).

(D) Flow cytometry plots show $tdTom^+$ progenitors (maroon), M□ (blue) and EC (green) in AGM/aorta at different ages. Pie charts show lineage breakdown of $tdTom^+$ cells (n=3-4/age).

(E) *Csf1r*^{MerCreMer} x *Rosa*^{GFP} mice were induced with TAM at E8.5 and analyzed at 12 w.

(F) GFP^+ CFU-M from 12 w aorta. Graph shows GFP^+ vs GFP^- status of CFU-M from aorta and BM, with results normalized to microglia (n=4).

(G) GFP^+ expression in 12 w aorta (mean % from n=4). No TAM control also shown.

(H) Graph shows numbers of GFP^+ progenitors, M□ and EC in 12 w aorta. Pie chart shows lineage breakdown of GFP^+ cells (n=4). Repeated measures ANOVA. Multiple test comparisons: *$p<0.05$ and †$p<0.01$ vs EC.

(I, J) Confocal microscopy of 12 w aorta shows (I) GFP^+ cells in adventitia (Ad) and (J) magnified examples of GFP^+ cells co-expressing CD31 in intima and CD68 and c-Kit in adventitia (arrows). L, lumen.

(K) FACS isolation and purity checks of YS-derived GFP^+ progenitors, M□ and EC from 12 w aorta.

(L) Wright-Giemsa staining of sorted GFP^+ populations, with results for total cell area, nuclear area and nuclear:cell area ratio (n=47-100 per cell type). Kruskal-Wallis tests. Multiple test comparisons: #p<0.0001 vs M□ and EC; †p<0.01 vs EC.

(M) CFU-M yield from GFP^+ progenitors, M□ and EC (four experiments, six aortas each). Friedman test.

Data summarized as mean±SD.

Scale bar, 100 μm.

Also see Figure S5.

Figure 4. Aortic CFU-M progenitors have endothelial and macrophage potential.

(A) Day 7 images after FACS sorted progenitors (Prog), macrophages (M□) or endothelial cells (EC) from 12 w aorta were cultured in Matrigel™. Arrows indicate cords. Graph shows total cord length (three experiments, six aortas each). Friedman test.

(B, C) Flow cytometry plots show fate of (B) EC and (C) progenitors in Matrigel™. Maroon, progenitors; blue, M□; green, EC.

(D) Example of aortic CFU-M from which progenitors produced cord networks (arrow) in Matrigel™.

(E) Flow cytometry plots and graph show fate of CFU-M derived progenitors in Matrigel™ (n=12). Green histogram, sample; grey, FMO control. Friedman test. Multiple comparison tests: *$p<0.05$ and #$p<0.0001$ for comparison to EC.

(F, G) Uptake of (F) DiI-oxLDL or (G) DiI-acLDL by aortic progenitors or their M□ or EC progeny produced in Matrigel™ (n=3). Paired t-tests.

(H) Total cord length and number of branches produced in Matrigel™ by progenitors from YS or aortic CFU-M from different aged C57BL/6 mice (n=3-4). One-way ANOVA. Multiple test comparisons: *$p<0.05$, †$p<0.01$, ‡$p<0.001$ and #$p<0.0001$ for comparison to 52 w.

(I) Adventitial sprouting assay using aortic progenitors from GFP mice added to adventitia-less aortic rings from C57BL/6 mice.

(J) Light and fluorescence microscopy and summarized results for adventitial sprouting with (+) and without (-) addition of GFP^+ progenitors (n=4-5). Unpaired t-test.

(K) Flow cytometry plots and graph show fate of GFP^+ aortic progenitors after 7 d of aortic ring assay (n=3). Friedman test. Multiple comparisons test: *$p<0.05$ for comparison to EC. Data summarized as mean±SD.

Scale bar, 100 µm.

Also see Figure S6.

Figure 5. CFU-M progenitors have endothelial-macrophage plasticity and vasculogenic capacity *in vivo*.

(A) 1° transfer of GFP^+ aortic progenitors after hindlimb ischemia surgery with two-week follow-up.

(B) Laser Doppler perfusion images on D0 and D14 after ischemia in mice receiving cell-free control (above) and progenitors (below). Graph shows results (n=6/gp). Mixed effects two-way ANOVA: $p<0.0001$ for time; $p=0.03$ for group; $p=0.005$ for time x group. Multiple comparison test: #$p<0.0001$ for Prog vs control.

(C) Flow cytometry plots and graph show fate of GFP^+ donor cells in recipient muscle (n=6). Maroon, progenitors (Prog); blue, macrophages (M□); green, endothelial cells (EC). Green histogram, sample; grey, FMO control. Repeated measures ANOVA. Multiple comparison test: *$p<0.05$ vs M□.

(D) Confocal microscopy of ischemic muscle shows neovessels lined by GFP^+CD31^+ EC (arrows) with cluster of GFP^+CD68^+ M□ (arrowhead) (above) and perfused with host $Ter119^+$ erythrocytes (below). L, lumen.

(E) 2° transfer of GFP^+ progenitors after hindlimb ischemia.

(F) Flow cytometry plots and graph show fate of GFP^+ donor cells after 2° transfer (n=3). Repeated measures ANOVA. Multiple comparison test: *$p<0.05$ vs Prog.

(G) 1° transfer of GFP^+ progenitors after hindlimb ischemia with eight-week follow-up.

(H) Flow cytometry plots and graph show fate of GFP^+ donor cells 8 w after 1° transfer (n=3). Repeated measures ANOVA. Multiple comparison test: *$p<0.05$ and †$p<0.01$ vs EC.

Data summarized as mean±SD.

Scale bar, 100 µm.

Also see Figure S6.

Figure 6. Regulatory effects of Angiotensin II on aortic EndoMac progenitors.

(A) Surface expression of ACE, ATR1 and ATR2 on progenitors from aortic CFU-M (n=3 12 w C57BL/6 mice).

(B) ACE expression on progenitors in C57BL/6 aortic digests (n=3).

(C) ACE expression on progenitors from E9.5 YS CFU-M (n=3).

(D) Normalized mRNA expression of *Agtr1* and *Agtr2* in progenitors from aortic CFU-M relative to same donor aortic digests (n=6 12w C57BL/6 mice). Wilcoxon signed rank tests.

(E) Aortic CFU-M yield with different concentrations of AngII, normalized to no AngII control (n=6 12 w C57BL/6 mice). Friedman test. Multiple comparison tests: *$p<0.05$, †$p<0.01$ vs control.

(F) Aortic CFU-M yield across serial passages in the presence or absence of 100 nM AngII (n=3 12 w C57BL/6 mice).

(G) Aortic CFU-M yield in the presence of inhibitors to ACE (Enalapril), AT1R (Losartan) and AT2R (PD123,319) normalized to control (n=3 12 w C57BL/6 mice). Friedman test. Multiple comparison tests: *$p<0.05$ vs control.

(H) Peritoneal transfer assay.

(I) Immunophenotype of GFP^+ aortic progenitors before intraperitoneal injection.

(J) Flow cytometry of peritoneal gavage shows macrophage fate of GFP^+ aortic progenitors after 72 h of daily injections of PBS, AngII or M-CSF.

(K) Number of macrophages produced by progenitors under different conditions (n=4). One-way ANOVA. Multiple comparisons test: *$p<0.05$ vs PBS.

(L-P) mRNA expression for select genes in aortic progenitors after treatment with AngII, normalized to no AngII control. Genes relate to (L) cell cycle; (M) progenitor/stem cell biology and self-renewal; (N) myelopoiesis; (O) macrophages; (P) endothelial biology and

angiogenesis. mRNA transcripts were first normalized to *β-actin*. Paired t-tests. n=3-4 12 w C57BL/6 mice.

Data summarized as mean±SD.

Figure 7. YS-derived EndoMac progenitors proliferate early during Angiotensin II-induced vascular inflammation

(A) PBS or AngII infusion in *Flt3*^{Cre} x *Rosa*$^{mT/mG}$ mice for 48 h.

(B-F) Graphs compare aortas from PBS and AngII groups for the numbers of Flt3^{+} and Flt3^{-}: (B) macrophages, (C) S-phase macrophages, (D) CFU-M yield, (E) progenitors and (F) S-phase progenitors (n=6/gp). Flow cytometry used for (B), (C), (E) and (F). Unpaired t-tests. Red p-values, Flt3^{-} comparisons; green p-values, Flt3^{+}.

(G) PBS or AngII infusion in E9.5 TAM-induced *Cx3cr1*$^{CreER\text{-}YFP}$ x *Rosa*^{tdTom} mice with BrdU pulse-chase.

(H) Flow cytometry of tdTom^{+} labeling in aortic digests. No TAM Cre control also shown. Percentages are mean tdTom^{+} (n=4). Graph shows number of tdTom^{+} cells in aortas. Two-way ANOVA: Interaction p=0.17, Time p=0.002, Group p=0.14. Group comparison: †p<0.01.

(I) Confocal microscopy of descending aorta after 48h of PBS or AngII. Graph shows % of tdTom^{+} cells in adventitia (Ad) (n=4, three sections each). Unpaired t-test. L, lumen. Nuclei stained with DAPI.

(J) tdTom^{+} aortic CFU-M yield (n=4). Two-way ANOVA: Interaction p<0.0001, Time p=0.0005, Group p<0.0001. Group comparisons: #p<0.0001, ‡p<0.001.

(K) Percentages of BrdU^{+} cells that were progenitors (Prog), macrophages (M□) or endothelial cells (EC) after 12 h of PBS or AngII and 1 h after BrdU (n=4).

(L) Flow cytometry of aortic digests after different durations of AngII, gated from tdTom^{+} cells. Maroon, Prog; Blue, M□; Green, EC.

(M-P) Numbers of BrdU^{+} tdTom^{+} (M) cells, (N) progenitors, (O) macrophages and (P) EC following BrdU pulse-chase for different durations of PBS or AngII infusion (n=4). p-values

are from one-way ANOVA for each treatment. ns, not significant. Multiple test comparisons: *$p<0.05$, †$p<0.01$, ‡$p<0.001$ vs 168 h.

Data summarized as mean±SD.

Scale bar, 100 μm. Also see Figure S7.

REFERENCES

Asahara, T., Masuda, H., Takahashi, T., Kalka, C., Pastore, C., Silver, M., Kearne, M., Magner, M., and Isner, J.M. (1999). Bone marrow origin of endothelial progenitor cells responsible for postnatal vasculogenesis in physiological and pathological neovascularization. Circ Res *85*, 221-228.

Auffray, C., Fogg, D.K., Narni-Mancinelli, E., Senechal, B., Trouillet, C., Saederup, N., Leemput, J., Bigot, K., Campisi, L., Abitbol, M., *et al.* (2009). CX3CR1+ CD115+ CD135+ common macrophage/DC precursors and the role of CX3CR1 in their response to inflammation. J Exp Med *206*, 595-606.

Aziz, A., Soucie, E., Sarrazin, S., and Sieweke, M.H. (2009). MafB/c-Maf deficiency enables self-renewal of differentiated functional macrophages. Science *326*, 867-871.

Bertrand, J.Y., Jalil, A., Klaine, M., Jung, S., Cumano, A., and Godin, I. (2005). Three pathways to mature macrophages in the early mouse yolk sac. Blood *106*, 3004-3011.

Boisset, J.C., van Cappellen, W., Andrieu-Soler, C., Galjart, N., Dzierzak, E., and Robin, C. (2010). In vivo imaging of haematopoietic cells emerging from the mouse aortic endothelium. Nature *464*, 116-120.

Bordt, E.A., Block, C.L., Petrozziello, T., Sadri-Vakili, G., Smith, C.J., Edlow, A.G., and Bilbo, S.D. (2020). Isolation of Microglia from Mouse or Human Tissue. STAR Protoc *1*, 100035.

Cahill, T.J., Sun, X., Ravaud, C., Villa Del Campo, C., Klaourakis, K., Lupu, I.E., Lord, A.M., Browne, C., Jacobsen, S.E.W., Greaves, D.R., *et al.* (2021). Tissue-resident macrophages regulate lymphatic vessel growth and patterning in the developing heart. Development *148*, dev194563.

Daugherty, A., Manning, M.W., and Cassis, L.A. (2000). Angiotensin II promotes atherosclerotic lesions and aneurysms in apolipoprotein E-deficient mice. J Clin Invest *105*, 1605-1612.

Dick, S.A., Macklin, J.A., Nejat, S., Momen, A., Clemente-Casares, X., Althagafi, M.G., Chen, J., Kantores, C., Hosseinzadeh, S., Aronoff, L., *et al.* (2019). Self-renewing resident cardiac macrophages limit adverse remodeling following myocardial infarction. Nat Immunol *20*, 29-39.

Elmore, M.R., Najafi, A.R., Koike, M.A., Dagher, N.N., Spangenberg, E.E., Rice, R.A., Kitazawa, M., Matusow, B., Nguyen, H., West, B.L., *et al.* (2014). Colony-stimulating factor 1 receptor signaling is necessary for microglia viability, unmasking a microglia progenitor cell in the adult brain. Neuron *82*, 380-397.

Ensan, S., Li, A., Besla, R., Degousee, N., Cosme, J., Roufaiel, M., Shikatani, E.A., El-Maklizi, M., Williams, J.W., Robins, L., *et al.* (2016). Self-renewing resident arterial macrophages arise from embryonic CX3CR1(+) precursors and circulating monocytes immediately after birth. Nat Immunol *17*, 159-168.

Epelman, S., Lavine, K.J., Beaudin, A.E., Sojka, D.K., Carrero, J.A., Calderon, B., Brija, T., Gautier, E.L., Ivanov, S., Satpathy, A.T., *et al.* (2014). Embryonic and adult-derived resident cardiac macrophages are maintained through distinct mechanisms at steady state and during inflammation. Immunity *40*, 91-104.

Fantin, A., Vieira, J.M., Gestri, G., Denti, L., Schwarz, Q., Prykhozhij, S., Peri, F., Wilson, S.W., and Ruhrberg, C. (2010). Tissue macrophages act as cellular chaperones for vascular anastomosis downstream of VEGF-mediated endothelial tip cell induction. Blood *116*, 829-840.

Feng, T., Gao, Z., Kou, S., Huang, X., Jiang, Z., Lu, Z., Meng, J., Lin, C.P., and Zhang, H. (2020). No Evidence for Erythro-Myeloid Progenitor-Derived Vascular Endothelial Cells in Multiple Organs. Circ Res *127*, 1221-1232.

Gentek, R., Ghigo, C., Hoeffel, G., Bulle, M.J., Msallam, R., Gautier, G., Launay, P., Chen, J., Ginhoux, F., and Bajenoff, M. (2018). Hemogenic Endothelial Fate Mapping Reveals Dual Developmental Origin of Mast Cells. Immunity *48*, 1160-1171 e1165.

Ghigo, C., Mondor, I., Jorquera, A., Nowak, J., Wienert, S., Zahner, S.P., Clausen, B.E., Luche, H., Malissen, B., Klauschen, F., *et al.* (2013). Multicolor fate mapping of Langerhans cell homeostasis. J Exp Med *210*, 1657-1664.

Ginhoux, F., Greter, M., Leboeuf, M., Nandi, S., See, P., Gokhan, S., Mehler, M.F., Conway, S.J., Ng, L.G., Stanley, E.R., *et al.* (2010). Fate mapping analysis reveals that adult microglia derive from primitive macrophages. Science *330*, 841-845.

Gomez Perdiguero, E., Klapproth, K., Schulz, C., Busch, K., Azzoni, E., Crozet, L., Garner, H., Trouillet, C., de Bruijn, M.F., Geissmann, F., *et al.* (2015). Tissue-resident macrophages originate from yolk-sac-derived erythro-myeloid progenitors. Nature *518*, 547-551.

Guilliams, M., De Kleer, I., Henri, S., Post, S., Vanhoutte, L., De Prijck, S., Deswarte, K., Malissen, B., Hammad, H., and Lambrecht, B.N. (2013). Alveolar macrophages develop from fetal monocytes that differentiate into long-lived cells in the first week of life via GM-CSF. J Exp Med *210*, 1977-1992.

Gurevich, D.B., Severn, C.E., Twomey, C., Greenhough, A., Cash, J., Toye, A.M., Mellor, H., and Martin, P. (2018). Live imaging of wound angiogenesis reveals macrophage orchestrated vessel sprouting and regression. EMBO J *37*, e97786.

Hashimoto, D., Chow, A., Noizat, C., Teo, P., Beasley, M.B., Leboeuf, M., Becker, C.D., See, P., Price, J., Lucas, D., *et al.* (2013). Tissue-resident macrophages self-maintain locally throughout adult life with minimal contribution from circulating monocytes. Immunity *38*, 792-804.

He, H., Xu, J., Warren, C.M., Duan, D., Li, X., Wu, L., and Iruela-Arispe, M.L. (2012). Endothelial cells provide an instructive niche for the differentiation and functional polarization of M2-like macrophages. Blood *120*, 3152-3162.

Hettinger, J., Richards, D.M., Hansson, J., Barra, M.M., Joschko, A.C., Krijgsveld, J., and Feuerer, M. (2013). Origin of monocytes and macrophages in a committed progenitor. Nat Immunol *14*, 821-30.

Hoeffel, G., Chen, J., Lavin, Y., Low, D., Almeida, F.F., See, P., Beaudin, A.E., Lum, J., Low, I., Forsberg, E.C., *et al.* (2015). C-Myb(+) erythro-myeloid progenitor-derived fetal monocytes give rise to adult tissue-resident macrophages. Immunity *42*, 665-678.

Hoeffel, G., and Ginhoux, F. (2018). Fetal monocytes and the origins of tissue-resident macrophages. Cell Immunol *330*, 5-15.

Huang, Y., Xu, Z., Xiong, S., Sun, F., Qin, G., Hu, G., Wang, J., Zhao, L., Liang, Y.X., Wu, T., *et al.* (2018). Repopulated microglia are solely derived from the proliferation of residual microglia after acute depletion. Nat Neurosci *21*, 530-540.

Jung, S., Aliberti, J., Graemmel, P., Sunshine, M.J., Kreutzberg, G.W., Sher, A., and Littman, D.R. (2000). Analysis of fractalkine receptor CX(3)CR1 function by targeted deletion and green fluorescent protein reporter gene insertion. Mol Cell Biol *20*, 4106-4114.

Iturri, L., Freyer, L., Biton, A., Dardenne, P., Lallemand, Y., and Gomez Perdiguero, E. (2021). Megakaryocyte production is sustained by direct differentiation from erythromyeloid progenitors in the yolk sac until midgestation. Immunity *54*, 1433-1446 e1435.

Karsunky, H., Merad, M., Cozzio, A., Weissman, I.L., and Manz, M.G. (2003). Flt3 ligand regulates dendritic cell development from Flt3+ lymphoid and myeloid-committed progenitors to Flt3+ dendritic cells in vivo. J Exp Med *198*, 305-313.

Kasaai, B., Caolo, V., Peacock, H.M., Lehoux, S., Gomez-Perdiguero, E., Luttun, A., and Jones, E.A. (2017). Erythro-myeloid progenitors can differentiate from endothelial cells and modulate embryonic vascular remodeling. Sci Rep *7*, 43817.

Kennedy, M., D'Souza, S.L., Lynch-Kattman, M., Schwantz, S., and Keller, G. (2007). Development of the hemangioblast defines the onset of hematopoiesis in human ES cell differentiation cultures. Blood *109*, 2679-2687.

Li, L., Jin, H., Xu, J., Shi, Y., and Wen, Z. (2011). Irf8 regulates macrophage versus neutrophil fate during zebrafish primitive myelopoiesis. Blood *117*, 1359-1369.

Lin, C., Datta, V., Okwan-Duodu, D., Chen, X., Fuchs, S., Alsabeh, R., Billet, S., Bernstein, K.E., and Shen, X.Z. (2011). Angiotensin-converting enzyme is required for normal myelopoiesis. FASEB J *25*, 1145-1155.

Manavski, Y., Lucas, T., Glaser, S.F., Dorsheimer, L., Gunther, S., Braun, T., Rieger, M.A., Zeiher, A.M., Boon, R.A., and Dimmeler, S. (2018). Clonal Expansion of Endothelial Cells Contributes to Ischemia-Induced Neovascularization. Circ Res *122*, 670-677.

Mass, E., Ballesteros, I., Farlik, M., Halbritter, F., Gunther, P., Crozet, L., Jacome-Galarza, C.E., Handler, K., Klughammer, J., Kobayashi, Y., *et al.* (2016). Specification of tissue-resident macrophages during organogenesis. Science *353*, aaf4238.

McGrath, K.E., Frame, J.M., Fegan, K.H., Bowen, J.R., Conway, S.J., Catherman, S.C., Kingsley, P.D., Koniski, A.D., and Palis, J. (2015). Distinct Sources of Hematopoietic Progenitors Emerge before HSCs and Provide Functional Blood Cells in the Mammalian Embryo. Cell Rep *11*, 1892-1904.

Medvinsky, A., Rybtsov, S., and Taoudi, S. (2011). Embryonic origin of the adult hematopoietic system: advances and questions. Development *138*, 1017-1031.

Moore, J.P., Vinh, A., Tuck, K.L., Sakkal, S., Krishnan, S.M., Chan, C.T., Lieu, M., Samuel, C.S., Diep, H., Kemp-Harper, B.K., *et al.* (2015). M2 macrophage accumulation in the aortic wall during angiotensin II infusion in mice is associated with fibrosis, elastin loss, and elevated blood pressure. Am J Physiol Heart Circ Physiol *309*, H906-917.

Morgan, K., Kharas, M., Dzierzak, E., and Gilliland, D.G. (2008). Isolation of early hematopoietic stem cells from murine yolk sac and AGM. J Vis Exp *16*, 789.

Murray, P.D.F. (1932). The development in vitro of blood of early chick embryo. Proc R Soc Lond Biol Sci *111*, 497-521.

Palis, J., Robertson, S., Kennedy, M., Wall, C., and Keller, G. (1999). Development of erythroid and myeloid progenitors in the yolk sac and embryo proper of the mouse. Development *126*, 5073-5084.

Patel, J., Seppanen, E.J., Rodero, M.P., Wong, H.Y., Donovan, P., Neufeld, Z., Fisk, N.M., Francois, M., and Khosrotehrani, K. (2017). Functional Definition of Progenitors Versus Mature Endothelial Cells Reveals Key SoxF-Dependent Differentiation Process. Circulation *135*, 786-805.

Perdiguero, E.G., Klapproth, K., Schulz, C., Busch, K., de Bruijn, M., Rodewald, H.R., and Geissmann, F. (2015). The Origin of Tissue-Resident Macrophages: When an Erythro-myeloid Progenitor Is an Erythro-myeloid Progenitor. Immunity *43*, 1023-1024.

Plein, A., Fantin, A., Denti, L., Pollard, J.W., and Ruhrberg, C. (2018). Erythro-myeloid progenitors contribute endothelial cells to blood vessels. Nature *562*, 223-228.

Potente, M., Gerhardt, H., and Carmeliet, P. (2011). Basic and therapeutic aspects of angiogenesis. Cell *146*, 873-887.

Psaltis, P.J., Harbuzariu, A., Delacroix, S., Witt, T.A., Holroyd, E.W., Spoon, D.B., Hoffman, S.J., Pan, S., Kleppe, L.S., Mueske, C.S., *et al.* (2012). Identification of a monocyte-predisposed hierarchy of hematopoietic progenitor cells in the adventitia of postnatal murine aorta. Circulation *125*, 592-603.

Psaltis, P.J., Puranik, A.S., Spoon, D.B., Chue, C.D., Hoffman, S.J., Witt, T.A., Delacroix, S., Kleppe, L.S., Mueske, C.S., Pan, S., *et al.* (2014). Characterization of a resident population of adventitial macrophage progenitor cells in postnatal vasculature. Circ Res *115*, 364-375.

Psaltis, P.J., and Simari, R.D. (2015). Vascular wall progenitor cells in health and disease. Circ Res *116*, 1392-1412.

Qian, B.Z., and Pollard, J.W. (2010). Macrophage diversity enhances tumor progression and metastasis. Cell *141*, 39-51.

Rateri, D.L., Howatt, D.A., Moorleghen, J.J., Charnigo, R., Cassis, L.A., and Daugherty, A. (2011). Prolonged infusion of angiotensin II in apoE(-/-) mice promotes macrophage recruitment with continued expansion of abdominal aortic aneurysm. Am J Pathol *179*, 1542-1548.

Reu, P., Khosravi, A., Bernard, S., Mold, J.E., Salehpour, M., Alkass, K., Perl, S., Tisdale, J., Possnert, G., Druid, H., *et al.* (2017). The Lifespan and Turnover of Microglia in the Human Brain. Cell Rep *20*, 779-784.

Samokhvalov, I.M., Samokhvalova, N.I., and Nishikawa, S. (2007). Cell tracing shows the contribution of the yolk sac to adult haematopoiesis. Nature *446*, 1056-1061.

Satoh, Y., Matsumura, I., Tanaka, H., Ezoe, S., Sugahara, H., Mizuki, M., Shibayama, H., Ishiko, E., Ishiko, J., Nakajima, K., *et al.* (2004). Roles for c-Myc in self-renewal of hematopoietic stem cells. J Biol Chem *279*, 24986-24993.

Schulz, C., Gomez Perdiguero, E., Chorro, L., Szabo-Rogers, H., Cagnard, N., Kierdorf, K., Prinz, M., Wu, B., Jacobsen, S.E., Pollard, J.W., *et al.* (2012). A lineage of myeloid cells independent of Myb and hematopoietic stem cells. Science *336*, 86-90.

Shen, X.Z., and Bernstein, K.E. (2011). The peptide network regulated by angiotensin converting enzyme (ACE) in hematopoiesis. Cell Cycle *10*, 1363-1369.

Sieweke, M.H., and Allen, J.E. (2013). Beyond stem cells: self-renewal of differentiated macrophages. Science *342*, 1242974.

Soucie, E.L., Weng, Z., Geirsdottir, L., Molawi, K., Maurizio, J., Fenouil, R., Mossadegh-Keller, N., Gimenez, G., VanHille, L., Beniazza, M., *et al.* (2016). Lineage-specific enhancers activate self-renewal genes in macrophages and embryonic stem cells. Science *351*, aad5510.

Stremmel, C., Schuchert, R., Wagner, F., Thaler, R., Weinberger, T., Pick, R., Mass, E., Ishikawa-Ankerhold, H.C., Margraf, A., Hutter, S., *et al.* (2018). Yolk sac macrophage progenitors traffic to the embryo during defined stages of development. Nat Commun *9*, 75.

Takata, K., Kozaki, T., Lee, C.Z.W., Thion, M.S., Otsuka, M., Lim, S., Utami, K.H., Fidan, K., Park, D.S., Malleret, B., *et al.* (2017). Induced-Pluripotent-Stem-Cell-Derived Primitive Macrophages Provide a Platform for Modeling Tissue-Resident Macrophage Differentiation and Function. Immunity *47*, 183-198 e186.

Taoudi, S., Gonneau, C., Moore, K., Sheridan, J.M., Blackburn, C.C., Taylor, E., and Medvinsky, A. (2008). Extensive hematopoietic stem cell generation in the AGM region via maturation of VE-cadherin+CD45+ pre-definitive HSCs. Cell Stem Cell *3*, 99-108.

Tay, T.L., Mai, D., Dautzenberg, J., Fernandez-Klett, F., Lin, G., Sagar, Datta, M., Drougard, A., Stempfl, T., Ardura-Fabregat, A., *et al.* (2017). A new fate mapping system reveals context-dependent random or clonal expansion of microglia. Nat Neurosci *20*, 793-803.

Toledo-Flores, D., Williamson, A., Schwarz, N., Fernando, S., Dimasi, C., Witt, T.A., Nguyen, T.M., Puranik, A.S., Chue, C.D., Delacroix, S., *et al.* (2019). Vasculogenic properties of adventitial Sca-1(+)CD45(+) progenitor cells in mice: a potential source of vasa vasorum in atherosclerosis. Sci Rep *9*, 7286.

van Furth, R., and Cohn, Z.A. (1968). The origin and kinetics of mononuclear phagocytes. J Exp Med *128*, 415-435.

Weinberger, T., Esfandyari, D., Messerer, D., Percin, G., Schleifer, C., Thaler, R., Liu, L., Stremmel, C., Schneider, V., Vagnozzi, R.J., *et al.* (2020). Ontogeny of arterial macrophages defines their functions in homeostasis and inflammation. Nat Commun *11*, 4549.

Wu, J., Montaniel, K.R., Saleh, M.A., Xiao, L., Chen, W., Owens, G.K., Humphrey, J.D., Majesky, M.W., Paik, D.T., Hatzopoulos, A.K., *et al.* (2016). Origin of Matrix-Producing Cells That Contribute to Aortic Fibrosis in Hypertension. Hypertension *67*, 461-468.

Yona, S., Kim, K.W., Wolf, Y., Mildner, A., Varol, D., Breker, M., Strauss-Ayali, D., Viukov, S., Guilliams, M., Misharin, A., *et al.* (2013). Fate mapping reveals origins and dynamics of monocytes and tissue macrophages under homeostasis. Immunity *38*, 79-91.

Zambidis, E.T., Park, T.S., Yu, W., Tam, A., Levine, M., Yuan, X., Pryzhkova, M., and Peault, B. (2008). Expression of angiotensin-converting enzyme (CD143) identifies and regulates primitive hemangioblasts derived from human pluripotent stem cells. Blood *112*, 3601-3614.

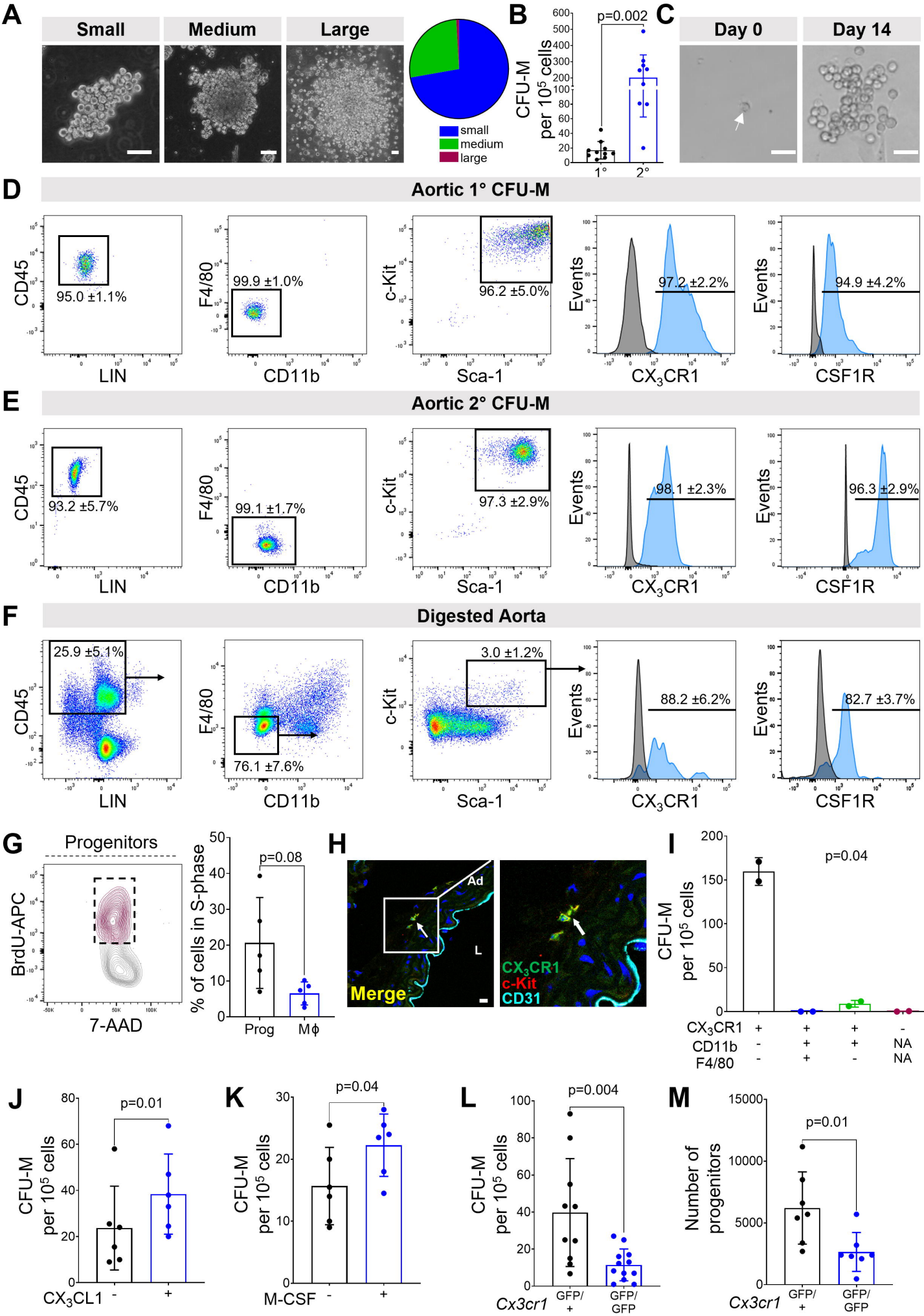
A
Small
Medium
Large
small
medium
large
B
p=0.002
CFU-M per 10^5 cells
1°
2°
C
Day 0
Day 14
D
Aortic 1° CFU-M
CD45
95.0 ±1.1%
LIN
F4/80
99.9 ±1.0%
CD11b
c-Kit
96.2 ±5.0%
Sca-1
Events
97.2 ±2.2%
CX3CR1
94.9 ±4.2%
CSF1R
E
Aortic 2° CFU-M
93.2 ±5.7%
99.1 ±1.7%
97.3 ±2.9%
98.1 ±2.3%
96.3 ±2.9%
F
Digested Aorta
25.9 ±5.1%
76.1 ±7.6%
3.0 ±1.2%
88.2 ±6.2%
82.7 ±3.7%
G
Progenitors
BrdU-APC
7-AAD
p=0.08
% of cells in S-phase
Prog
Mϕ
H
Ad
L
Merge
CX3CR1
c-Kit
CD31
I
p=0.04
CFU-M per 10^5 cells
CX3CR1
CD11b
F4/80
NA
J
p=0.01
CX3CL1
K
p=0.04
M-CSF
L
p=0.004
Cx3cr1
GFP/+
GFP/GFP
M
p=0.01
Number of progenitors

Figure 1

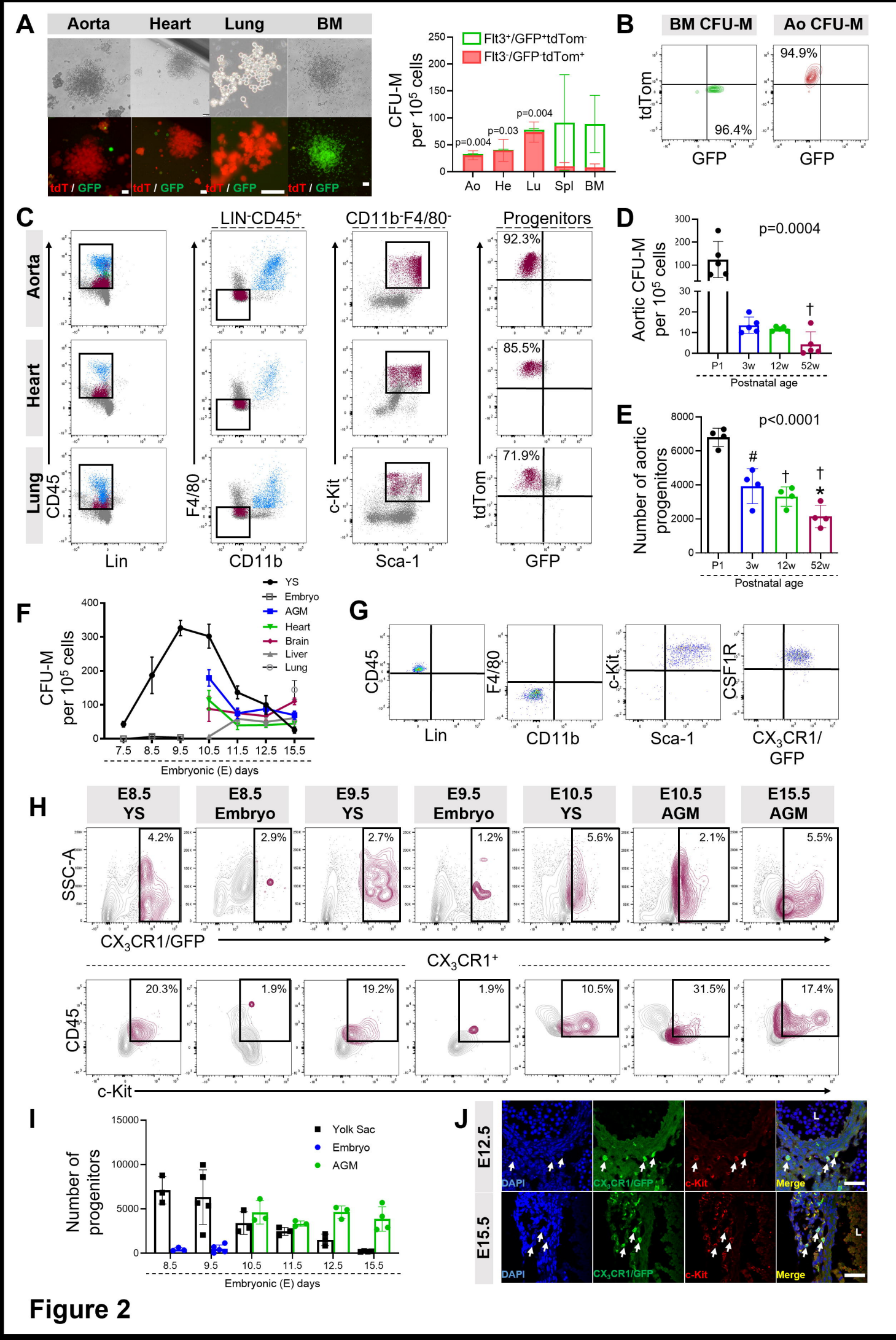
A
Aorta
Heart
Lung
BM
tdT / GFP
CFU-M per 10^5 cells
Flt3+/GFP+tdTom-
Flt3-/GFP-tdTom+
p=0.004
p=0.03
p=0.004
Ao
He
Lu
Spl
BM
B
BM CFU-M
Ao CFU-M
tdTom
GFP
96.4%
94.9%
C
Aorta
Heart
Lung
CD45
Lin
LIN-CD45+
F4/80
CD11b
CD11b-F4/80-
c-Kit
Sca-1
Progenitors
tdTom
GFP
92.3%
85.5%
71.9%
D
Aortic CFU-M per 10^5 cells
p=0.0004
P1
3w
12w
52w
Postnatal age
E
Number of aortic progenitors
p<0.0001
P1
3w
12w
52w
Postnatal age
F
CFU-M per 10^5 cells
YS
Embryo
AGM
Heart
Brain
Liver
Lung
Embryonic (E) days
G
CD45
Lin
F4/80
CD11b
c-Kit
Sca-1
CSF1R
CX3CR1/GFP
H
E8.5 YS
E8.5 Embryo
E9.5 YS
E9.5 Embryo
E10.5 YS
E10.5 AGM
E15.5 AGM
SSC-A
CX3CR1/GFP
CX3CR1+
4.2%
2.9%
2.7%
1.2%
5.6%
2.1%
5.5%
CD45
c-Kit
20.3%
1.9%
19.2%
1.9%
10.5%
31.5%
17.4%
I
Number of progenitors
Yolk Sac
Embryo
AGM
Embryonic (E) days
J
E12.5
E15.5
DAPI
CX3CR1/GFP
c-Kit
Merge
L

Figure 2

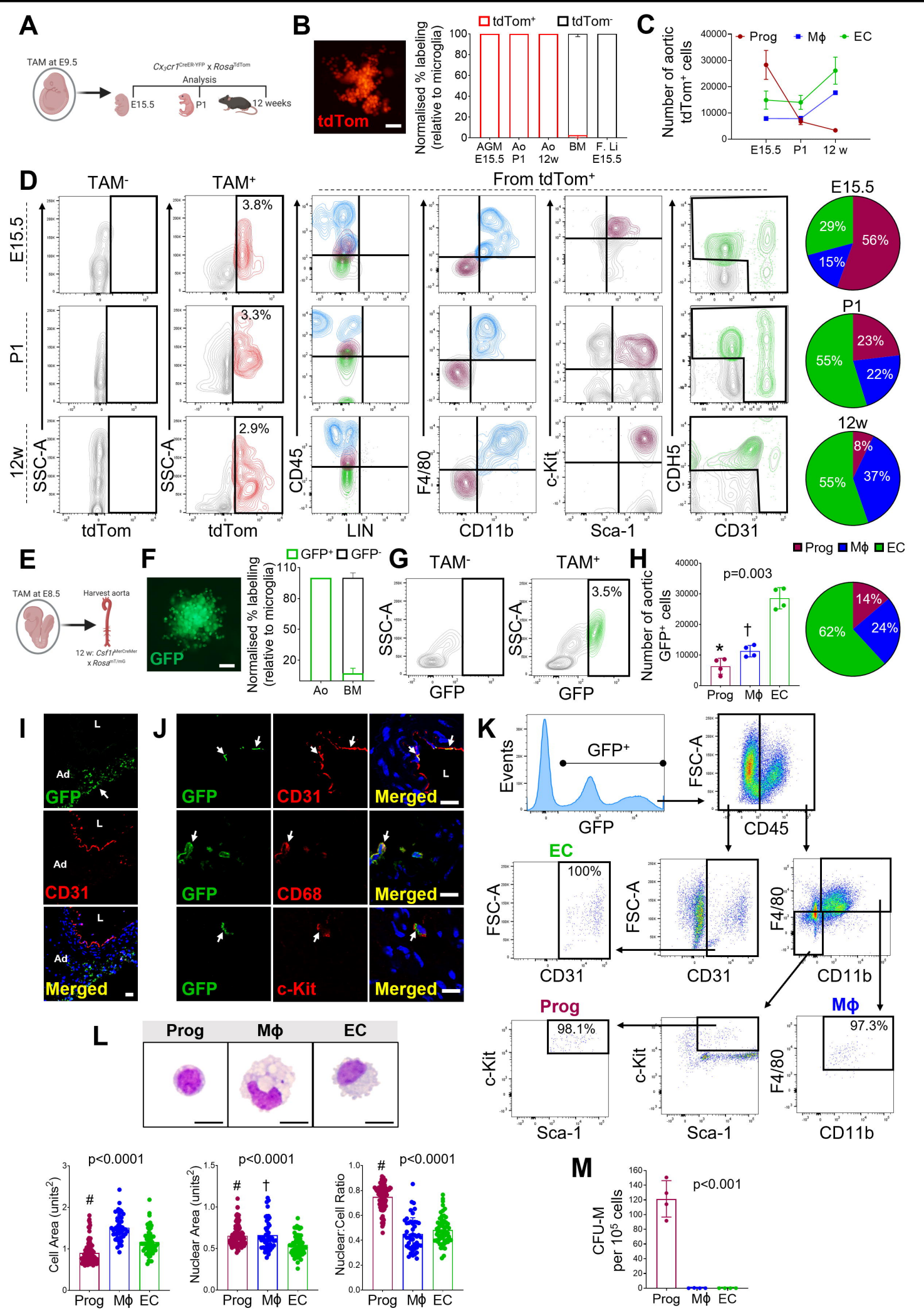
A
TAM at E9.5
Cx3cr1CreER-YFP x RosaTdTom
Analysis
E15.5
P1
12 weeks
B
tdTom
tdTom+
tdTom-
Normalised % labeling (relative to microglia)
AGM E15.5
Ao P1
Ao 12w
BM
F. Li E15.5
C
Number of aortic tdTom+ cells
Prog
Mϕ
EC
E15.5
P1
12 w
D
TAM-
TAM+
From tdTom+
E15.5
P1
12w
3.8%
3.3%
2.9%
SSC-A
tdTom
CD45
LIN
F4/80
CD11b
c-Kit
Sca-1
CDH5
CD31
56%
29%
15%
23%
55%
22%
8%
37%
55%
E
TAM at E8.5
Harvest aorta
12 w: Csf1MerCreMer x RosamT/mG
F
GFP
GFP+
GFP-
Normalised % labelling (relative to microglia)
Ao
BM
G
TAM-
TAM+
3.5%
SSC-A
GFP
H
Number of aortic GFP+ cells
p=0.003
Prog
Mϕ
EC
14%
24%
62%
I
L
Ad
GFP
CD31
Merged
J
GFP
CD31
CD68
c-Kit
Merged
K
Events
GFP+
GFP
FSC-A
CD45
EC
100%
CD31
CD11b
F4/80
Prog
98.1%
Mϕ
97.3%
c-Kit
Sca-1
L
Prog
Mϕ
EC
p<0.0001
Cell Area (units2)
Nuclear Area (units2)
Nuclear:Cell Ratio
M
CFU-M per 10^5 cells
p<0.001

Figure 3

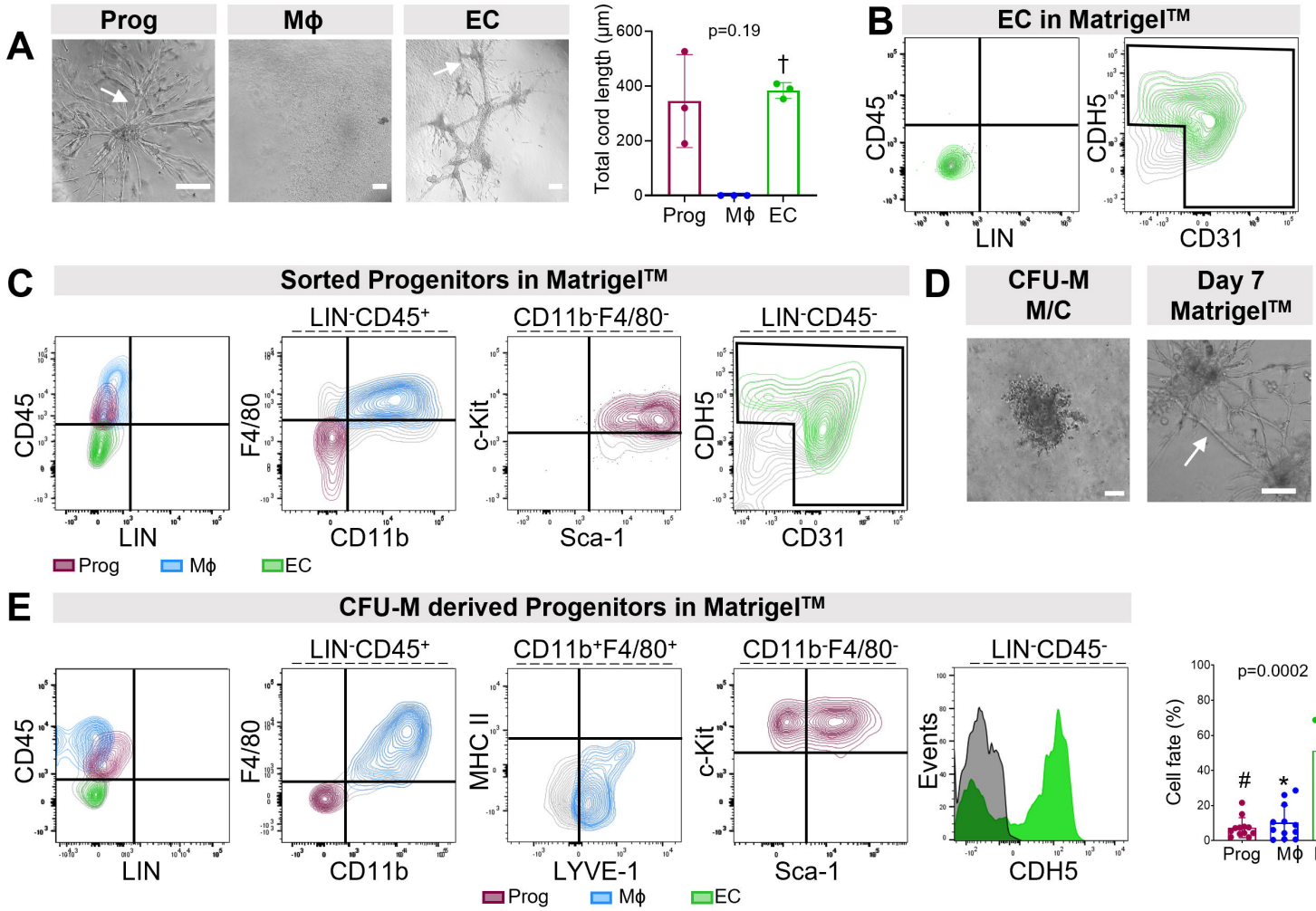
A
Prog
Mϕ
EC
Total cord length (µm)
p=0.19
Prog
Mϕ
EC
B
EC in Matrigel™
CD45
LIN
CDH5
CD31
C
Sorted Progenitors in Matrigel™
LIN-CD45+
CD11b-F4/80-
LIN-CD45-
CD45
LIN
F4/80
CD11b
c-Kit
Sca-1
CDH5
CD31
Prog
Mϕ
EC
D
CFU-M M/C
Day 7 Matrigel™
E
CFU-M derived Progenitors in Matrigel™
LIN-CD45+
CD11b+F4/80+
CD11b-F4/80-
LIN-CD45-
CD45
LIN
F4/80
CD11b
MHC II
LYVE-1
c-Kit
Sca-1
Events
CDH5
Cell fate (%)
p=0.0002
Prog
Mϕ
EC

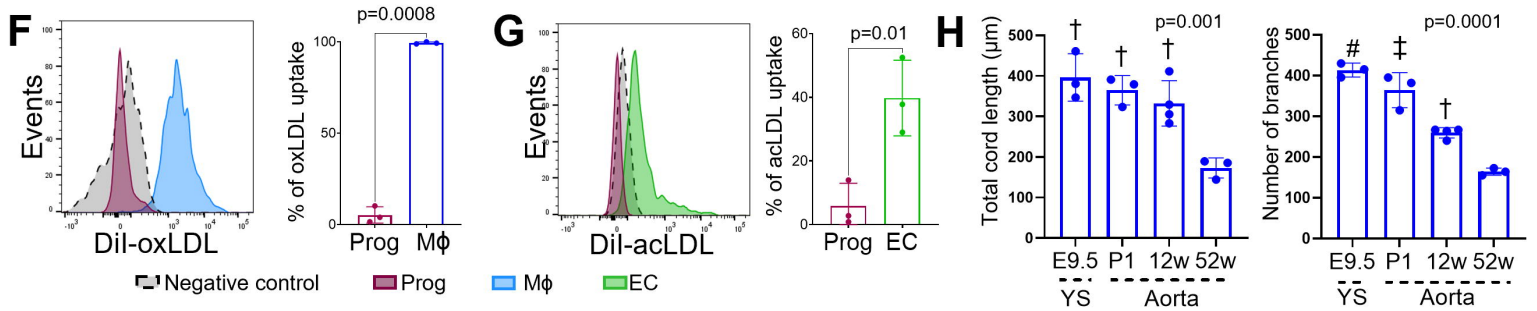
F
Events
DiI-oxLDL
% of oxLDL uptake
p=0.0008
Prog
Mϕ
G
Events
DiI-acLDL
% of acLDL uptake
p=0.01
Prog
EC
Negative control
Prog
Mϕ
EC
H
Total cord length (µm)
p=0.001
E9.5
P1
12w
52w
YS
Aorta
Number of branches
p=0.0001
E9.5
P1
12w
52w
YS
Aorta

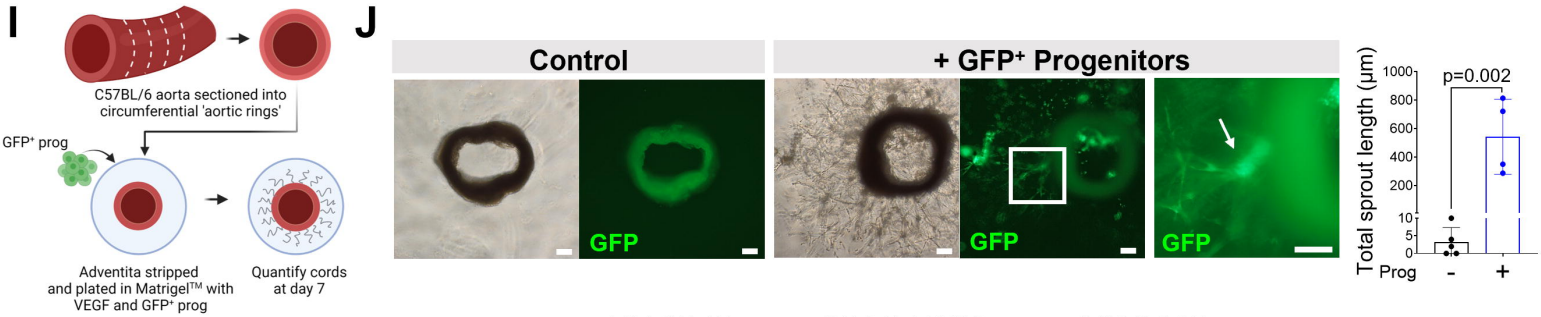
I
C57BL/6 aorta sectioned into circumferential 'aortic rings'
GFP+ prog
Adventita stripped and plated in Matrigel™ with VEGF and GFP+ prog
Quantify cords at day 7
J
Control
+ GFP+ Progenitors
GFP
GFP
GFP
Total sprout length (µm)
p=0.002
Prog
-
+

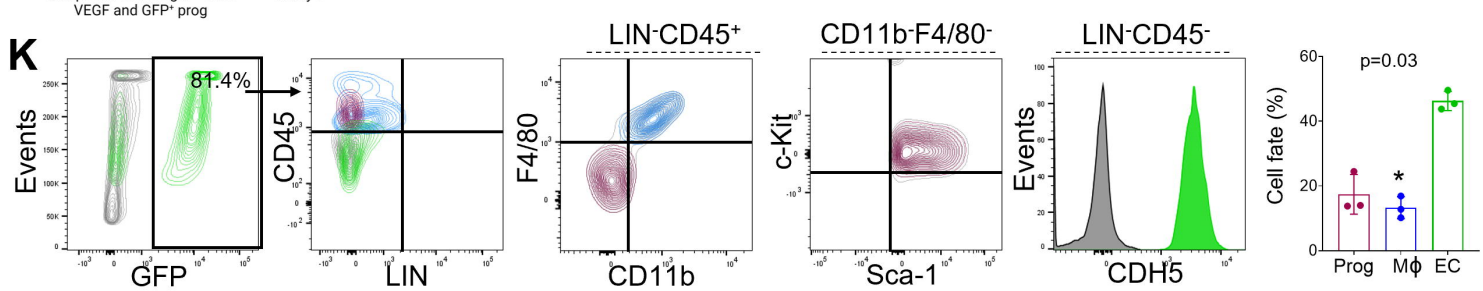
K
Events
81.4%
GFP
CD45
LIN
LIN-CD45+
F4/80
CD11b
CD11b-F4/80-
c-Kit
Sca-1
LIN-CD45-
Events
CDH5
Cell fate (%)
p=0.03
Prog
Mϕ
EC

Figure 4

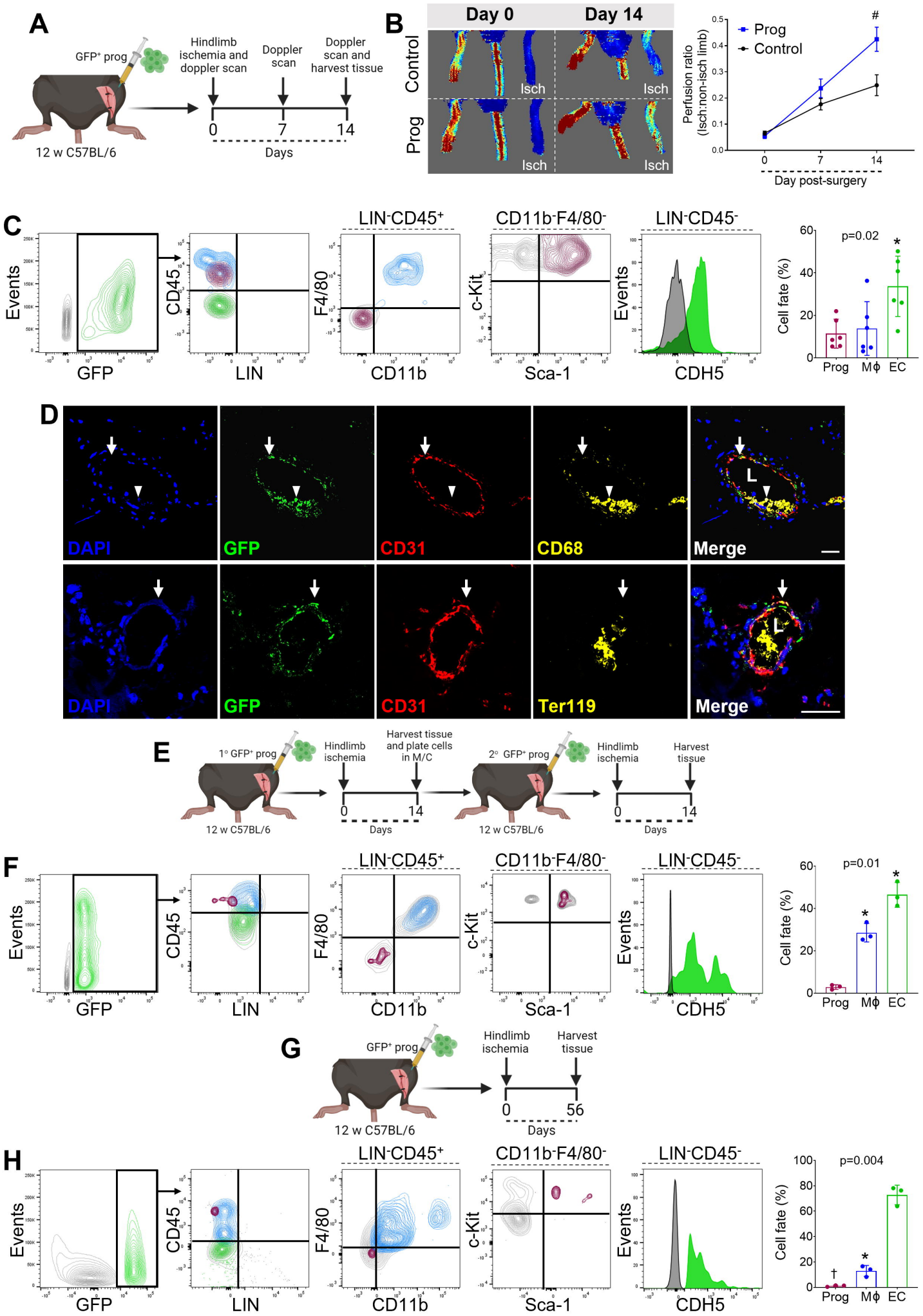
A
GFP+ prog
12 w C57BL/6
Hindlimb ischemia and doppler scan
Doppler scan
Doppler scan and harvest tissue
0
7
14
Days
B
Day 0
Day 14
Control
Prog
Isch
Perfusion ratio (Isch:non-isch limb)
Prog
Control
#
Day post-surgery
C
LIN-CD45+
CD11b-F4/80-
LIN-CD45-
Events
GFP
CD45
LIN
F4/80
CD11b
c-Kit
Sca-1
CDH5
Cell fate (%)
p=0.02
*
Prog
Mϕ
EC
D
DAPI
GFP
CD31
CD68
Merge
L
Ter119
E
1° GFP+ prog
Hindlimb ischemia
Harvest tissue and plate cells in M/C
2° GFP+ prog
Hindlimb ischemia
Harvest tissue
12 w C57BL/6
Days
F
p=0.01
G
GFP+ prog
Hindlimb ischemia
Harvest tissue
56
H
p=0.004
†

Figure 5

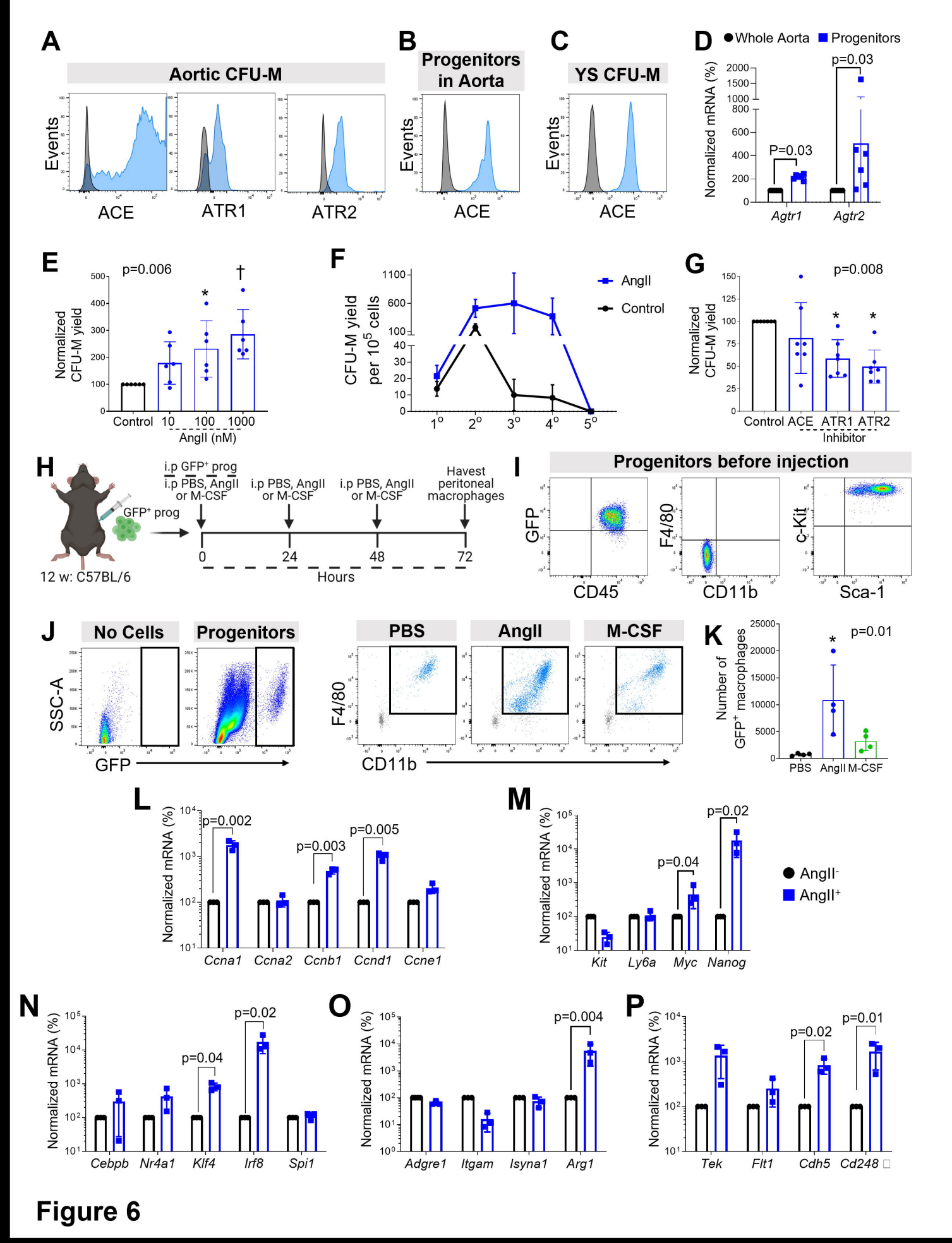
A
Aortic CFU-M
Events
ACE
ATR1
ATR2
B
Progenitors in Aorta
Events
ACE
C
YS CFU-M
Events
ACE
D
Whole Aorta
Progenitors
Normalized mRNA (%)
p=0.03
P=0.03
Agtr1
Agtr2
E
p=0.006
Normalized CFU-M yield
Control
10
100
1000
AngII (nM)
F
CFU-M yield per 10^5 cells
AngII
Control
1°
2°
3°
4°
5°
G
p=0.008
Normalized CFU-M yield
Control
ACE
ATR1
ATR2
Inhibitor
H
12 w: C57BL/6
GFP+ prog
i.p GFP+ prog
i.p PBS, AngII or M-CSF
i.p PBS, AngII or M-CSF
i.p PBS, AngII or M-CSF
Havest peritoneal macrophages
0
24
48
72
Hours
I
Progenitors before injection
GFP
CD45
F4/80
CD11b
c-Kit
Sca-1
J
No Cells
Progenitors
SSC-A
GFP
PBS
AngII
M-CSF
F4/80
CD11b
K
p=0.01
Number of GFP+ macrophages
PBS
AngII
M-CSF
L
Normalized mRNA (%)
p=0.002
p=0.003
p=0.005
Ccna1
Ccna2
Ccnb1
Ccnd1
Ccne1
M
Normalized mRNA (%)
p=0.02
p=0.04
Kit
Ly6a
Myc
Nanog
AngII-
AngII+
N
Normalized mRNA (%)
p=0.02
p=0.04
Cebpb
Nr4a1
Klf4
Irf8
Spi1
O
Normalized mRNA (%)
p=0.004
Adgre1
Itgam
Isyna1
Arg1
P
Normalized mRNA (%)
p=0.02
p=0.01
Tek
Flt1
Cdh5
Cd248

Figure 6

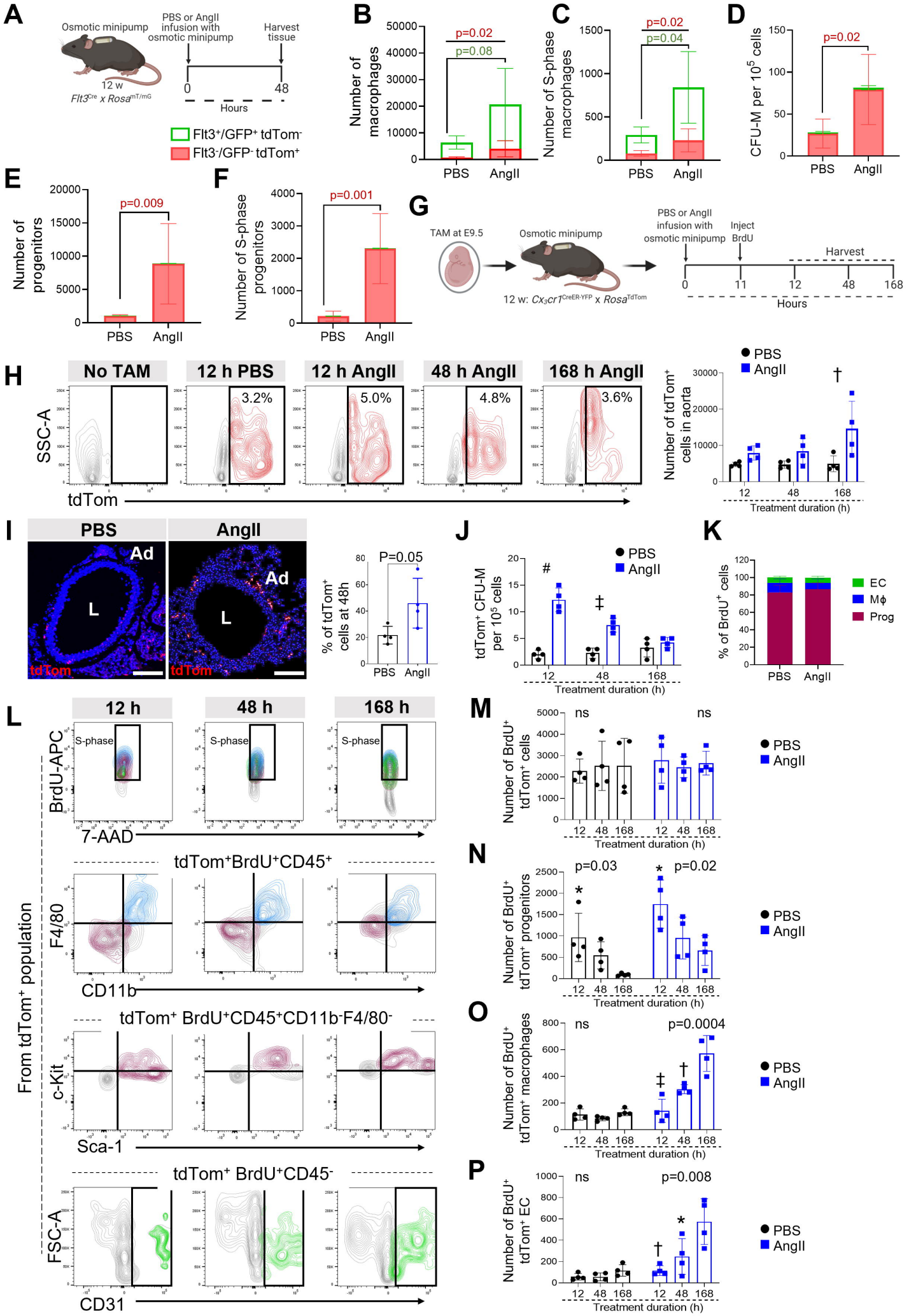
A
Osmotic minipump
PBS or AngII infusion with osmotic minipump
Harvest tissue
12 w
Flt3Cre x RosamT/mG
0
48
Hours
Flt3+/GFP+ tdTom-
Flt3-/GFP- tdTom+
B
Number of macrophages
p=0.02
p=0.08
PBS
AngII
C
Number of S-phase macrophages
p=0.02
p=0.04
D
CFU-M per 10^5 cells
p=0.02
E
Number of progenitors
p=0.009
F
Number of S-phase progenitors
p=0.001
G
TAM at E9.5
Osmotic minipump
12 w: Cx3cr1CreER-YFP x RosaTdTom
PBS or AngII infusion with osmotic minipump
Inject BrdU
Harvest
0
11
12
48
168
Hours
H
No TAM
12 h PBS
12 h AngII
48 h AngII
168 h AngII
3.2%
5.0%
4.8%
3.6%
SSC-A
tdTom
Number of tdTom+ cells in aorta
PBS
AngII
Treatment duration (h)
I
PBS
AngII
Ad
L
tdTom
% of tdTom+ cells at 48h
P=0.05
J
tdTom+ CFU-M per 10^5 cells
Treatment duration (h)
K
% of BrdU+ cells
EC
Mϕ
Prog
L
12 h
48 h
168 h
S-phase
BrdU-APC
7-AAD
tdTom+BrdU+CD45+
F4/80
CD11b
tdTom+ BrdU+CD45+CD11b-F4/80-
c-Kit
Sca-1
tdTom+ BrdU+CD45-
FSC-A
CD31
From tdTom+ population
M
Number of BrdU+ tdTom+ cells
ns
ns
Treatment duration (h)
N
Number of BrdU+ tdTom+ progenitors
p=0.03
p=0.02
O
Number of BrdU+ tdTom+ macrophages
ns
p=0.0004
P
Number of BrdU+ tdTom+ EC
ns
p=0.008

Figure 7